



UvA-DARE (Digital Academic Repository)

The discovery of GluA3-dependent synaptic plasticity

Renner, M.C.

Publication date

2016

Document Version

Final published version

[Link to publication](#)

Citation for published version (APA):

Renner, M. C. (2016). *The discovery of GluA3-dependent synaptic plasticity*. [Thesis, fully internal, Universiteit van Amsterdam]. Uitgeverij BOXPress.

General rights

It is not permitted to download or to forward/distribute the text or part of it without the consent of the author(s) and/or copyright holder(s), other than for strictly personal, individual use, unless the work is under an open content license (like Creative Commons).

Disclaimer/Complaints regulations

If you believe that digital publication of certain material infringes any of your rights or (privacy) interests, please let the Library know, stating your reasons. In case of a legitimate complaint, the Library will make the material inaccessible and/or remove it from the website. Please Ask the Library: <https://uba.uva.nl/en/contact>, or a letter to: Library of the University of Amsterdam, Secretariat, P.O. Box 19185, 1000 GD Amsterdam, The Netherlands. You will be contacted as soon as possible.

Chapter 3

Motor learning requires Purkinje cell synaptic potentiation through activation of AMPA-receptor subunit GluA3

Nicolas Gutierrez-Castellanos, Carla M. Da Silva-Matos, Kuikui Zhou, Cathrin B. Canto, Maria C. Renner, Linda Koene, Rolf Sprengel, Helmut W. Kessels and Chris I. De Zeeuw.

Submitted.

ABSTRACT

Synaptic plasticity at pyramidal cells in the hippocampus mediated by trafficking of GluA1-containing AMPA-receptors contributes to the formation of declarative memories. Synaptic plasticity also controls procedural memory formation, yet it is unclear to what extent GluA1- and GluA3-containing AMPA-receptors are critical for this form of learning in the cerebellar cortex. Here we show that long-term potentiation (LTP) at the parallel fiber to Purkinje cell synapse and adaptation of the vestibulo-ocular reflex do not depend on GluA1, but on GluA3-containing AMPA-receptors. In contrast to hippocampal GluA1-dependent LTP, this form of GluA3-dependent LTP does not require trafficking of receptors, but rather changes in open-channel probability mediated by an increase of cyclic AMP and activation of the protein directly activated by cAMP (Epac). Setting it apart from hippocampal learning, we conclude that vestibulo-cerebellar motor learning is the first form of memory acquisition shown to depend on GluA3-dependent synaptic potentiation through an increase in channel conductance.

INTRODUCTION

Plasticity mediated by synaptic trafficking of α -amino-3-hydroxy-5-methyl-4-isoxazolepropionic acid - type glutamate receptors (AMPA-receptors) plays an important role in the acquisition of declarative memories (Kessels and Malinow, 2009). Ionotropic AMPARs drive fast excitatory neuronal activity and can consist of four different subunits named GluA1 to GluA4. In mature hippocampal pyramidal cells, most AMPARs are hetero-oligomers composed of either GluA1/GluA2 or GluA2/GluA3 subunits and the subunit composition dictates which role AMPARs play in synaptic plasticity (Shi et al., 2001). In the hippocampus, cortex and amygdala, both LTP and learning depend on the trafficking of GluA1-containing AMPARs to synapses (Makino and Malinow, 2009; Nedeleescu et al., 2010; Rumpel et al., 2005; Takahashi et al., 2003), whereas GluA3-containing AMPARs contribute little to synaptic currents or plasticity (Adamczyk et al., 2012, Meng et al., 2003, Humeau et al., 2007). Interestingly, emotional states such as fear can transiently activate synaptic GluA3-plasticity in CA1-neurons of the hippocampus via an increase in intracellular cyclic AMP (Chapter 2), yet the role of GluA3-plasticity in adaptive behavior remains to be established.

Here, we sought to unravel the potential role of GluA1- and/or GluA3-containing AMPARs in cerebellar motor learning. Unlike the rich insight in the role of AMPARs in declarative memory formation in the hippocampus, relatively little is known about their role in procedural memory formation in the cerebellum. AMPAR plasticity is involved in parallel fiber to Purkinje cell (PF-PC) synapses reflecting the expression of LTP or long-term depression (LTD) (Takegawa and Yuzaki, 2005; Steinberg et al., 2006), but the full functional significance of and the precise molecular pathways underlying this plasticity remain to be further elucidated (Gao et al., 2012). In addition, the roles of GluA1- and/or GluA3-containing AMPARs in plasticity of PCs have hardly been studied (Bats et al., 2013; Douyard et al., 2007; Takegawa and Yuzaki, 2005).

We found that adaptation of compensatory eye movements, which serves to stabilize gaze and which is one of the most widely studied forms of cerebellar motor learning (Anzai et al., 2010, Nguyen-Vu et al., 2013; Schonewille et al., 2011), depends on GluA3-containing AMPARs. These GluA3-containing AMPARs in PCs are critical for the induction and expression of PF-PC LTP, not by trafficking of receptors, but by a change in conductance and open probability. This form of plasticity requires activation of Epac through an increase of cyclic AMP. Together, these findings do not only show that GluA3 is crucial for cerebellar potentiation and learning, but also that it evokes its actions of plasticity through a novel mechanism.

RESULTS

Cerebellar motor learning depends on GluA3, but not on GluA1

Global deficiency of GluA2 leads to ataxia and causes severe motor performance deficits (Gerlai et al., 1998). In contrast, mice that lack either AMPAR subunit GluA1 or GluA3 (GluA1-KO and GluA3-KO) display intact basic motor behavior, as judged by their ability to stabilize their gaze and/or images on their retina with respect to a moving visual field (i.e. optokinetic reflex or OKR; Figure S1A), with respect to their head movements (i.e. the vestibulo-ocular reflex in the dark or VOR; Figure S1B), or with respect to a combination of the two as occurs in daily life (i.e. VOR in the light or VORL; Figure S1C). Far more challenging is the test for VOR phase-reversal adaptation, which involves cerebellum-dependent motor learning (Gutierrez-Castellanos et al., 2013). During this paradigm mice learn to shift the phase of their VOR following sinusoidal visuovestibular mismatch stimulation, in which the visual

stimulus moves in the same direction in-phase with the vestibular stimulus, yet at a greater amplitude (Figure 1A). After 5 days of training mature wild-type mice adapt their eye movement in the same direction as the body instead of the innate contraversive compensation (phase 0°); they learned to shift their VOR in the dark by 159° out of the perfect 180° . When we subjected littermate GluA1-deficient mice to this phase-reversal adaptation paradigm, they reached final average phase shifts of 162° (GluA1-KO vs. WT: $p=0.13$; Figure 1B), indicating that GluA1-containing AMPARs are dispensable for VOR adaptation. In contrast, GluA3-deficient mice showed striking deficits in shifting the phase of their VOR in the dark; they showed a final phase shift of only 35° (GluA3-KO vs. WT: $p<0.001$; Figure 1B). If we look not

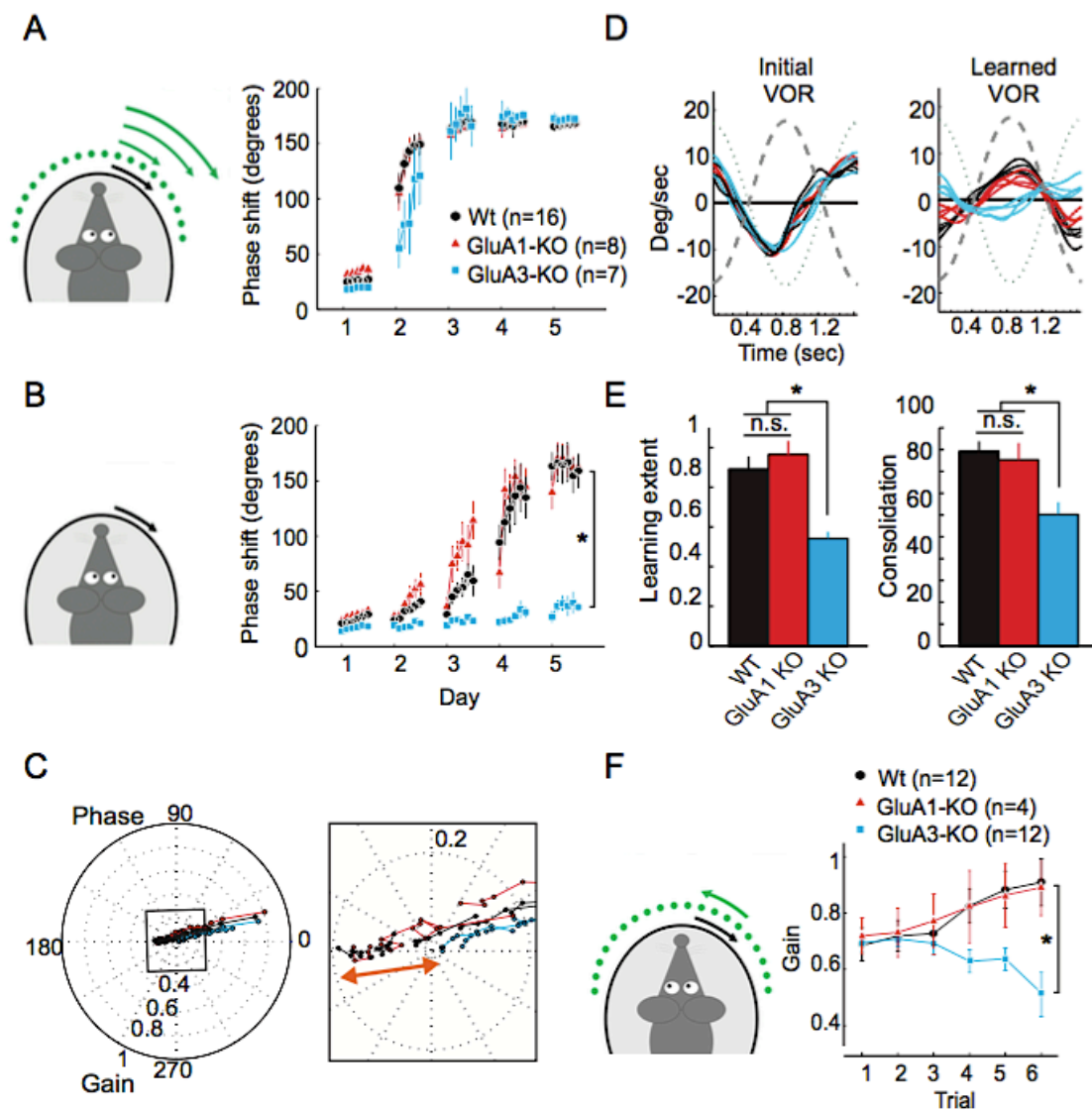


Figure 1. GluA3 is required for oculomotor learning.

(A) Eye movement phase values during visuo-vestibular mismatch training of adult (3-5 months of age) wild-type (black), GluA1-KO (red) and GluA3-KO mice (blue), showing a similar ability to follow the training signal. (B) Phase values of VOR adaptation catch trials for

the same groups of mice show significantly impaired motor learning in GluA3-KO mice compared to both GluA1-KO and WT groups during the phase reversal task. (C) Polar plot of gain and phase data combined with the data plotted in B shows a common learning trajectory and comparable initial gain for WTs (black line), GluA3-KOs (blue), and GluA1-KOs (red). Inset: the final VOR reached after 5 days of training is amplified to visualize the magnitude of the gain difference between the groups tested. (D) GluA3-KOs (blue line) were unable to reverse their VOR phase compared with WT (black) and GluA1-KOs (red). Four representative eye velocity traces per group compare the initial VOR before (left) and after (right) the mismatch training (left). (E) Both learning extent and consolidation during the phase reversal task are significantly smaller in GluA3-KO mice compared to WT and GluA1-KO mice (T2-test $p < 0.05$). (F) Gain increase learning also reveals deficits in GluA3-KO, but not GluA1-KO and WTs. Error bars indicate SEM, * indicates $p < 0.05$.

only at the oculomotor phase but at the learning trajectory extent (as explained in Figure S2A), we observe that whereas the initial performances of VOR catch learning trials were not significantly different for any of the 3 groups tested, the final performances of GluA3-KO after 5 days of training were significantly different from those of both wild-type littermates ($p=0.01$, Figure 1C) and GluA1-KO mice ($p=0.01$). Accordingly, the vector of total learning extent per mouse, which equals the distance between the initial (1st recording, 1st day, Figure S2) and final VOR performance coordinate throughout the 5-day spanning phase-reversal paradigm, was significantly smaller for GluA3-KO mice compared to wild-type and GluA1-KO mice (both p values < 0.01 ; Figures 1D and 1E). Moreover, the consolidation rate of learning, which equals the ratio between the total learning extent and the ideal learning extent with no overnight memory loss between training days (Figure S2A), was also significantly lower in GluA3-KO compared to both GluA1-KO and wild-type littermates (both p values < 0.01 ; Figure 1E). Importantly, all groups of mice performed equally during the visually-driven vestibular training trials over the 5 days of training (all p values > 0.05 ; Figure 1A), indicating that the learning deficits in GluA3-KO did not directly result from a poor response to the visuo-vestibular training signal, but rather an impaired ability to maintain this learned vestibular response in the absence of the visual cue (Figure 1B). Finally, when we applied an out-of-phase visuovestibular training paradigm to increase the gain rather than to reverse the phase, GluA3-KO showed yet again severe learning deficits ($p < 0.01$ for final catch trials), whereas GluA1-KO and wild-types performed equally well (all p values > 0.05 ; Figure 1F). These experiments suggest that GluA3-containing AMPARs contribute to cerebellum-dependent motor learning.

GluA3 is required to induce LTP, but not LTD, at PF-PC synapses

Purkinje cells are the sole output of the cerebellar cortex. It has been previously shown that synaptic plasticity at parallel fiber afferents crucially contribute to motor learning (Schonewille et al., 2010). To investigate the contribution of GluA1- and GluA3-containing AMPARs to basal transmission, we recorded spontaneous miniature excitatory synaptic currents (mEPSCs) of PCs in cerebellar slices from 4-6 week old GluA1-KO, GluA3-KO and wild-type littermates (Figure 2A). At this age GluA3-KO mice have similar motor learning deficits as at mature age (Figure S2D). In PCs that lack both GluA1 and GluA3 mEPSC events were virtually absent (Figure 2B), indicating that PCs mainly express GluA1- and GluA3-containing AMPARs. The average amplitude and frequency of mEPSCs in GluA1-deficient PCs were not significantly different ($p=0.4$ and $p=0.2$ respectively) from those in wild-type PCs (Figure 2B). However, in the absence of GluA3 both the average mEPSC amplitude ($p<0.01$) and frequency ($p<0.05$) were significantly lower than those in wild-type PCs. This low basal transmission was neither reflected in structural changes at the level of spine densities of proximal or distal PC dendrites (Figure S3) nor was it compensated by increased synaptic currents from kainate receptors (Figure S5).

A reduced basal transmission in GluA3-deficient PC synapses can either be a cause or a consequence of impaired synaptic plasticity. We investigated LTD and LTP at PF to PC synapses, the two main cellular models for motor learning, using whole-cell recordings. LTD was induced in PCs by pairing PF stimulation with a depolarizing voltage-clamp step, mimicking climbing fiber input (Linden, 2001; see methods). The magnitude of LTD in PCs of both GluA1-KO and GluA3-KO was indistinguishable from that in PCs of wild-type littermates (GluA1-KO vs. wild-type: $p=0.4$; GluA3-KO vs. wild-type: $p=0.2$) (Figure 2C). These data are in line with other studies showing that GluA2 is the key subunit for AMPAR internalization and therefore for LTD induction (Steinberg et al., 2006, Schonewille et al., 2011). Next, we induced LTP by tetanic stimulation of PF to PC input without depolarizing voltage-clamp steps (Figure 2D). In line with previous studies reporting that LTP at PF to PC synapses is expressed at the postsynaptic site after 1 Hz stimulation of PFs (Lev-Ram et al., 2002), we did not find significant changes in paired-pulse facilitation (PPF) of the evoked EPSCs after LTP induction ($p=0.4$, compared to baseline). This stimulation protocol produced LTP in GluA1-KO PCs reliably and indistinguishably from wild-type PCs, but failed to do so in PCs that lack GluA3 (Figure 2D). These experiments demonstrate that PF to PC LTP requires GluA3-containing AMPARs.

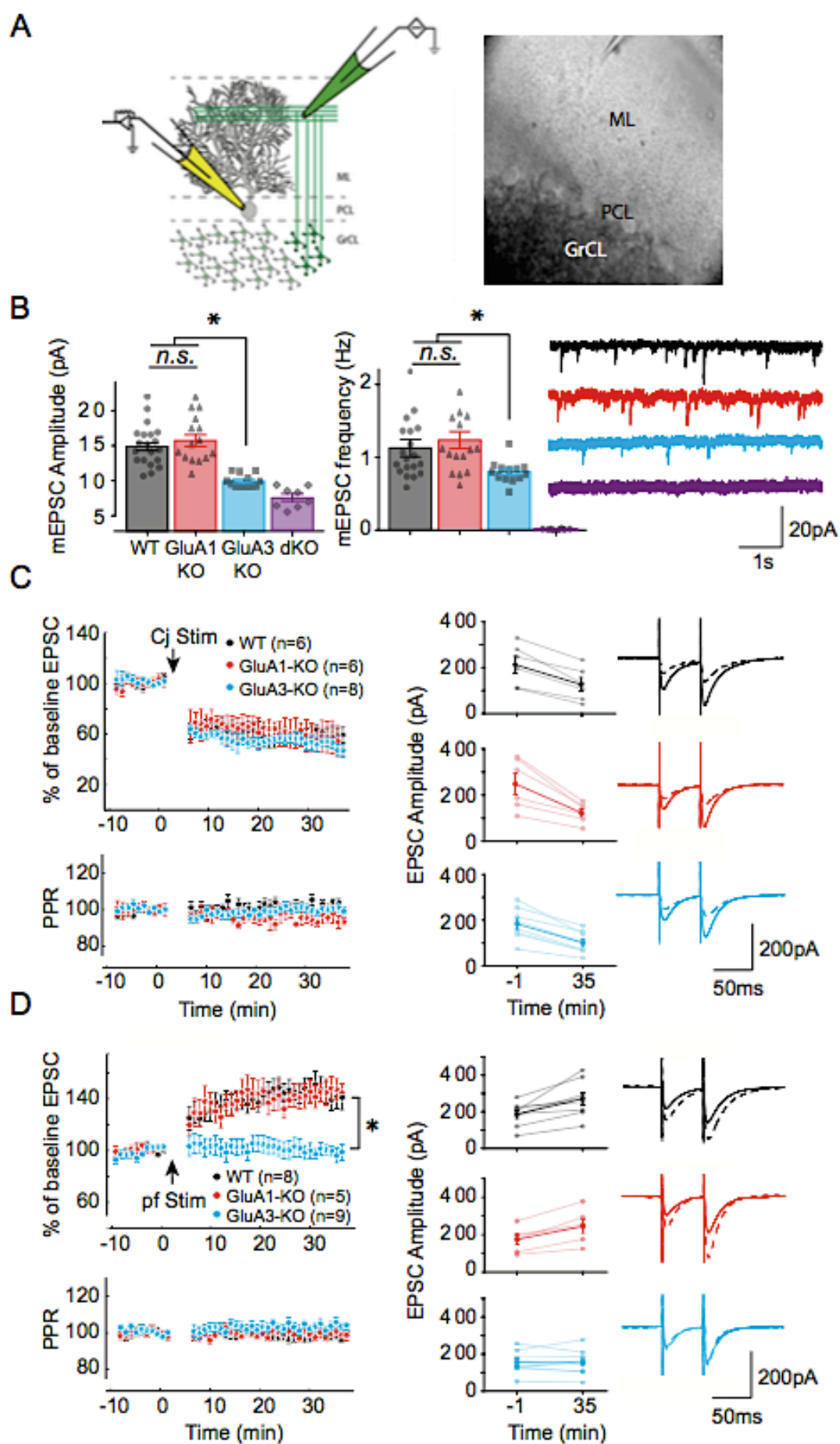


Figure 2. GluA3 is required for PF to PC LTP, but not LTD.

(A) Scheme of cerebellar cortical circuitry (Left) and representative picture of the in vitro preparation (right) showing positions of recording electrode (yellow) at PC soma and stimulus electrode (green) at parallel fiber beam. ML, PCL and GrCL indicate molecular layer, Purkinje cell layer, and granule cell layer, respectively. (B) The lack of GluA3 reduced basal transmission in that mEPSC amplitude (left panel) and frequency (middle panel) of both single GluA3-KO PCs (blue bar) and double GluA1/3-KO PCs (purple bar) were significantly reduced compared to those in WT PCs (black bar) and single GluA1-KO PCs (red bar). Right panel shows corresponding raw traces of mEPSCs. (C) Both GluA1-KOs (red) and GluA3-KOs (blue) show similar cerebellar synaptic weakening after LTD induction compared to WT littermates (black) (top left panel) with unchanged PPR over time (bottom left panel). EPSC magnitude was held in a comparable range for all cases to prevent potential bias due to differential basal synaptic strength (middle panels). Representative traces of paired EPSCs before (solid lines) and after LTD induction (dashed lines) (right panels, matched genotype color code). (D) GluA3-KO PCs show severe deficits in PF to PC LTP compared with WTs and GluA1-KOs with no changes in PPR or baseline EPSC magnitude. Representative traces of paired EPSCs before (solid lines) and after LTP induction (dashed lines) (same configuration as in B). Error bars indicate SEM, * indicates $p < 0.05$.

GluA3-dependent synaptic potentiation involves a cAMP-driven change in channel conductance

What is the molecular mechanism underlying GluA3-dependent LTP of PF-PC synapses? In Chapter 2 we show that GluA3-containing AMPARs can strengthen synapses of CA1-neurons upon an intracellular rise in cyclic AMP (cAMP) (Chapter 2). To test whether GluA3-dependent synaptic plasticity in PCs also depends on cAMP-signaling, we administered the adenylyl cyclase activator forskolin to PCs of GluA3-KO brain slices and compared the effects to those in wild-type slices and GluA1-KO slices (Figure 3A). Whereas forskolin produced on average a two-fold potentiation in PF-evoked EPSCs in both wild-type and GluA1-KO PCs ($230 \pm 25\%$ and $215 \pm 35\%$, respectively), it failed to induce synaptic potentiation in PCs that lack GluA3 ($95 \pm 10\%$; $p < 0.001$ GluA3-KO vs. wild-type). Importantly, AMPAR potentiation also occurred in wild-type PCs when local stimulation with $1 \mu\text{M}$ AMPA was used while blocking PFs with TTX ($189 \pm 17\%$, $p < 0.001$; Figure 3B), highlighting its postsynaptic nature (Chen and Regehr, 1997). These data indicate that a rise in the cellular level of cAMP can cause potentiation of PF-PC synaptic inputs through activation of GluA3-containing AMPARs.

We next examined whether cAMP-driven synaptic potentiation is a result of synaptic trafficking of GluA3-containing AMPARs. To assess whether forskolin increases GluA3 levels on the cell surface of spines, we performed time-lapse 2-photon imaging of PCs in cultured organotypic cerebellar slices infected with Sindbis virus to

acutely express GluA3 subunits fused to Super Ecliptic pHluorin (SEP). SEP is a pH-sensitive variant of GFP that shows a reduction in fluorescence upon rapid application of acidic (pH5) ACSF (Figure 3E). As a consequence, in our case the majority of SEP fluorescence at dendritic regions was derived from GluA3 located at the cell surface (Makino and Malinow, 2009). To test whether GluA3 trafficking can be detected with this method, we first triggered LTD chemically by adding the metabotropic mGluR1 receptor agonist DHPG to induce internalization of AMPARs (Linden, 2001). Indeed, application of DHPG to wild-type PCs expressing SEP-GluA3 produced a significant decrease in synaptic strength ($p=0.004$ for amplitude and $p=0.04$ for frequency; Figure 3C) and in SEP fluorescence at spines ($p<0.0001$; i.e. Figures 3D-F), which is in line with the endocytosis of AMPARs that occurs during the expression of depression at the PF-PC synapse (Wang and Linden, 2000). However, although washing-in forskolin significantly increased synaptic currents in SEP-GluA3 expressing PCs ($p=0.04$ for amplitude and $p<0.0001$ for frequency; Figure 3C), it failed to induce any acute change in SEP-fluorescence at PC spines ($0.03\pm 0.015\%$ change, $p=0.4$; Figures 3D-F), suggesting that the cAMP-driven synaptic potentiation does not require an insertion of GluA3-containing AMPARs at the surface of spines. We next assessed whether we could detect the trafficking of endogenous AMPARs to the cell surface upon forskolin treatment. Given that the available GluA3-antibodies display insufficient specificity, we tested endogenous GluA2 surface levels as indicators of GluA2/GluA3 heteromers by immunostaining for GluA2 following intracardiac perfusions of wild-type mice with or without forskolin. Although forskolin perfusion induced a significant 1.3 fold increase in mEPSC amplitude in PCs ($p=0.003$, Figure S6B), it did not significantly ($p=0.5$) modify surface levels of endogenous GluA2 in the molecular layer of the cerebellum (Figure S6A). Together, these data suggest GluA3-plasticity does not involve trafficking of GluA3-containing AMPARs to the cell surface or to synapses upon a rise in cAMP.

Since trafficking of AMPARs into the PC surface membrane did not appear to be the dominant mechanism that underlies GluA3-dependent synaptic potentiation at the PF to PC synapse, we next considered a change in channel properties. We resolved single-channel AMPA mediated currents by clamping a single AMPAR in cell-attached mode at the cell body of either GluA1-KO or GluA3-KO PCs with the recording pipette containing near-saturating concentrations of AMPA (Armstrong et al., 2002). GluA1-containing AMPARs at the surface of GluA3-KO PC cell bodies stochastically reached open states 1, 2 and 3 indicating binding of 2, 3 and 4 ligands, respectively, and displayed similar conductance levels and open-channel probability

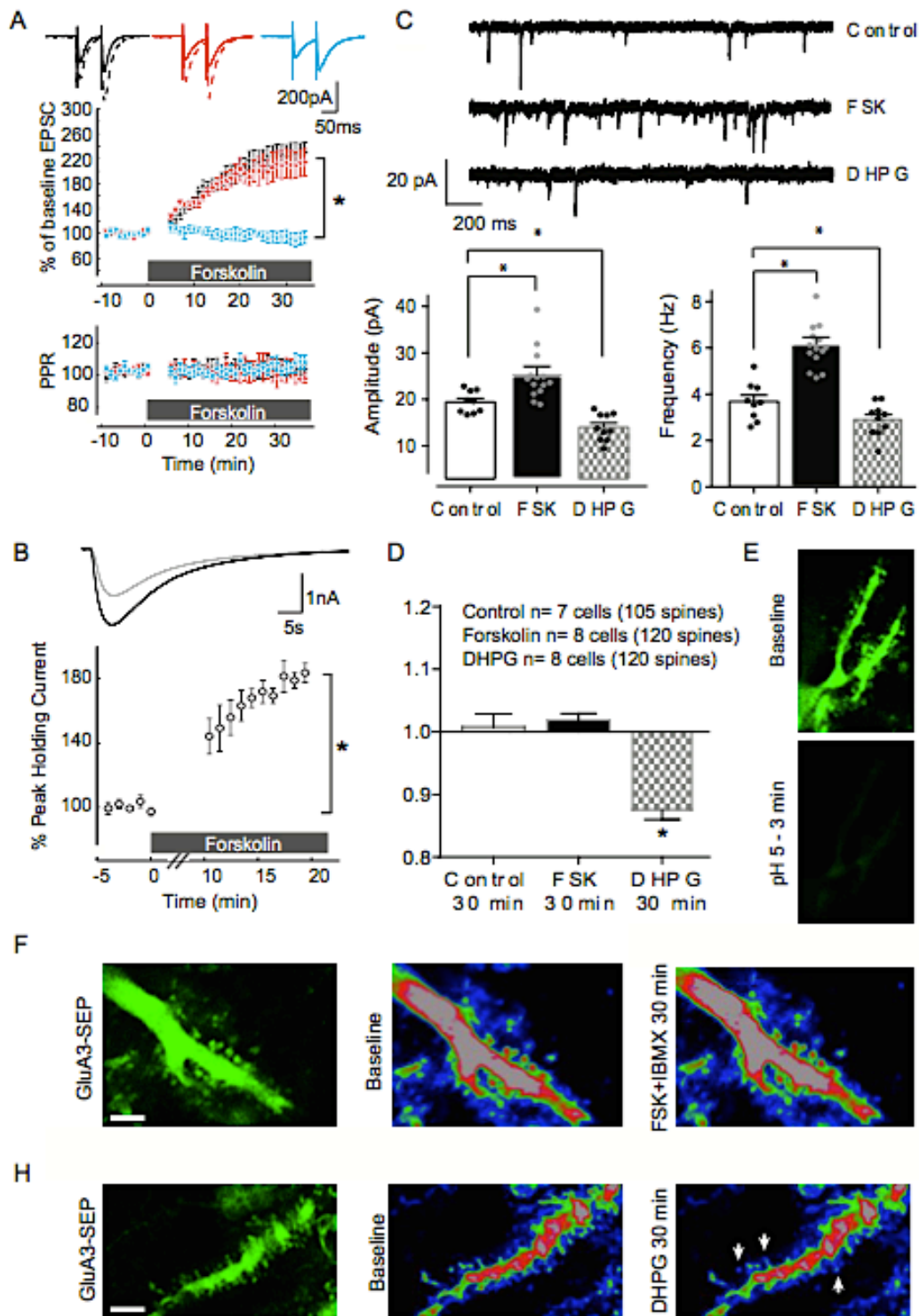


Figure 3. Rising cAMP levels produces GluA3-dependent synaptic potentiation without AMPARs trafficking.

(A) Wash-in of 50 μ M forskolin causes synaptic potentiation that depends on GluA3 (blue), but not GluA1 (red). Top, middle and bottom panel show example traces, normalized EPSC amplitude and paired pulsed ratio (PPR), respectively. (B) Enhancement of currents evoked by local puffs of 1 μ M AMPA at the molecular layer following forskolin application can also occur in the presence of TTX blocking PF input. (C) Forskolin produces a significant increase and DHPG a significant decrease of mEPSCs amplitude and frequency in GluA3-SEP

transfected PCs in organotypic slices. (D) Despite the synaptic potentiation, the ratio of spine fluorescence intensity after over before FSK application (FSK - middle bar) showed no significant increase of GluA3-SEP compared to the spines in which the drug was not applied (Control - left bar). However, DHPG application significantly reduced GluA3-SEP in PC spines in accordance to the observed synaptic depression. (E) Lowering the extracellular pH produced a drastic reduction of GluA3-SEP fluorescence intensity corroborating its pH sensitivity. (F) Left column: Z-max projection of a stack of pictures showing a representative GluA3-SEP transfected PC. Top row: Example picture of a PC dendrite expressing GluA3-SEP (left), pictures before (middle) and after (right) FSK application were color coded according to the fluorescence intensity to improve the visualization of, in this case, the absence of changes of surface GluA3-SEP over time. Bottom row: Example picture of a PC dendrite expressing GluA3-SEP (left). Color coded pictures before (middle) and after (right) DHPG application reveal a significant reduction in synaptic GluA3-SEP over time. Error bars indicate SEM, * indicates $p < 0.05$.

in the presence or absence of forskolin application (Figure S7). In contrast, GluA3-containing AMPARs on cell bodies of GluA1-KO PCs produced the vast majority of their openings in the first and lower conductance state (O1) under basal conditions (Figure 4A,B), indicating that only two out of the four ligand binding domains (LBDs) present in the AMPAR tetramer are activated by AMPA. After application of forskolin the behavior of GluA3-containing AMPARs changed strikingly and produced a significantly higher amount of openings in state O3 and O4 similar to GluA1-containing AMPARs (Figures 4A, B and E). The average duration of the openings was unchanged ($p=0.4$, 0.13 and 0.09 for O1, O2 and O3 respectively) (Figure 4C), but an increase of the absolute frequency of the openings caused shortening of the closed state dwell-time (Figure 6C) and thus a significant net increase of the open probability ($p < 0.0001$, Figure 4E). Although forskolin did not change the conductance level of any of the open states ($p=0.7$, 0.14 and 0.15 for O1, O2 and O3 respectively, Figure 4D), the higher relative fraction of events in the highly conductive open states O3 and O4 caused a significant increase ($p < 0.0001$) in the overall conductance of cAMP stimulated GluA3 channels (Figure 4B,D). These experiments suggest that a rise in intracellular cAMP produces synaptic potentiation by increasing the open-channel probability of the GluA3 subunit. Interestingly, this type of GluA3-dependent plasticity, which depends on receptor property changes rather than trafficking, was also found at hippocampal synapses (Chapter 2), indicating a unified, novel mechanistic model for GluA3-dependent synaptic plasticity.

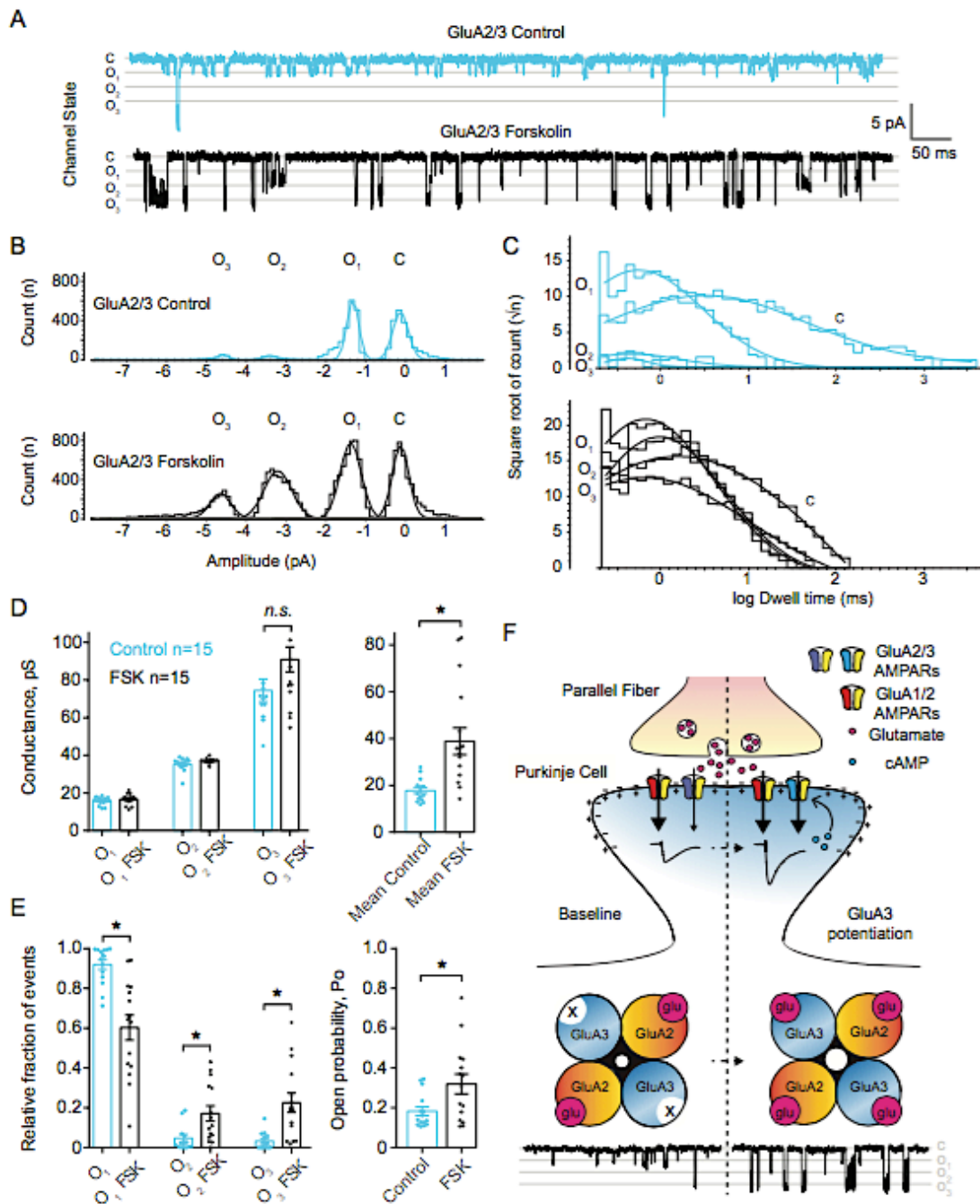


Figure 4. GluA3-plasticity occurs through cAMP-dependent changes of single channel conductance and open probability.

(A) Example traces of cell attached single channel recordings of GluA2/3 AMPARs in PCs of GluA1-KO mice. It can be observed that whereas under basal conditions (blue) the vast majority of their openings occur at the low conductance level (O1), in the presence of forskolin the amount of openings in the higher conductance levels (O2-3) notoriously increase (black). (B) Count versus amplitude histograms of the events detected in the representative recordings showed in A, illustrate the uneven distribution of events across the different conductance levels in the absence (blue) or presence (black) of forskolin. (C) The opening duration (dwell time) of the same events showed in A and B was unchanged after forskolin application. However the duration of the closed state time was reduced suggesting a net increase in the total number of openings produced by GluA2/3 channels in the presence of forskolin. (D) Overall quantification of GluA2/3 single channel recordings show that the

conductance of the 3 different opening states was unchanged in the presence of forskolin, however the uneven distribution of events as shown in B produce a significantly increased average conductance of GluA2/3 AMPAR currents after cAMP activation. (E) Forskolin significantly changed the distribution of GluA2/3 AMPARs events as shown by a significant decrease of events in O1 state and a significant increase in events at O2 and O3 states. The reduction of the closed state time showed in C was translated in a significant increase of the open channel probability. (F) Despite having functional GluA1/2 and GluA2/3 AMPARs, the model for GluA1 subunit specific LTP prevailing in the hippocampus, cortex or amygdala is not valid in PF to PC synapses. Note that absolute numbers of both subsets of AMPARs are unchanged upon LTP induction, whereas the GluA2/3 AMPARs are activated by cAMP signaling enhancing their channel conductance and therefore increasing the current generated in potentiated synapses. This model describes for the first time a form of GluA3 dependent LTP. Error bars indicate SEM, * indicates $p < 0.05$.

GluA3-mediated plasticity is induced via cAMP-mediated Epac activation

To further elucidate the molecular mechanism underlying GluA3-dependent plasticity, we aimed to identify the intermediary factor that translates a rise in cAMP into synaptic potentiation of GluA3-containing AMPARs. Protein kinase A (PKA) is activated by a rise in cAMP and exerts cAMP-dependent synaptic effects (Lev-Ram et al., 2002; Sokolova et al., 2006). However, blocking PKA in wild-type PCs with KT5720 (5 μ M; $n=6$) or H89 (20 μ M; $n=6$) did not have any significant effect on synaptic potentiation induced by forskolin ($215 \pm 20\%$ with KT5720 and $235 \pm 19\%$ with H89; $p=0.7$ and $p=0.9$, respectively) (Figure 5A). We next assessed the involvement of Epac (exchange proteins directly activated by cAMP, a.k.a. Rap guanine-nucleotide-exchange factor) as an alternative cAMP-dependent pathway that can trigger synaptic changes (Gekel and Neher, 2008; Woolfrey et al., 2009). The blockade of Epac with its selective antagonist ESI-05 (Tsalkova et al., 2012) did not reduce basal transmission at PF-PC synapses (Fig. 6H), but it effectively prevented the forskolin-induced synaptic potentiation in wild-type PCs ($p=0.89$ vs. baseline and $p < 0.0001$ vs. without ESI-05; Figure 5A). To assess whether Epac activation is not only necessary, but also sufficient to cause GluA3-dependent synaptic potentiation, we investigated the impact of the selective Epac activator 8-CPT-2Me-cAMP (8CPT). Adding 20 μ M 8CPT to the intracellular recording solution produced synaptic potentiation by $185 \pm 17\%$ compared to baseline in wild-type PCs ($n=12$, $p < 0.0001$; Figure 5B), but not in GluA3-deficient PCs ($n=7$, $100 \pm 5\%$; $p=0.8$; Figure 5B). In addition, the postsynaptic application of 8CPT increased the amplitude and frequency of PC mEPSCs ($p < 0.001$ and $p < 0.002$, respectively; Figure 5C,D) and did not change the PPF ratio ($104 \pm 5\%$, Figure 5B). These experiments indicate that a rise in cAMP triggers synaptic potentiation through Epac-mediated activation of postsynaptic GluA3-containing AMPARs. This Epac-driven activation of GluA3-

containing AMPARs was not limited to those located at synapses. Outside-out patches excised from wild-type PC somata produced a peak current of approximately

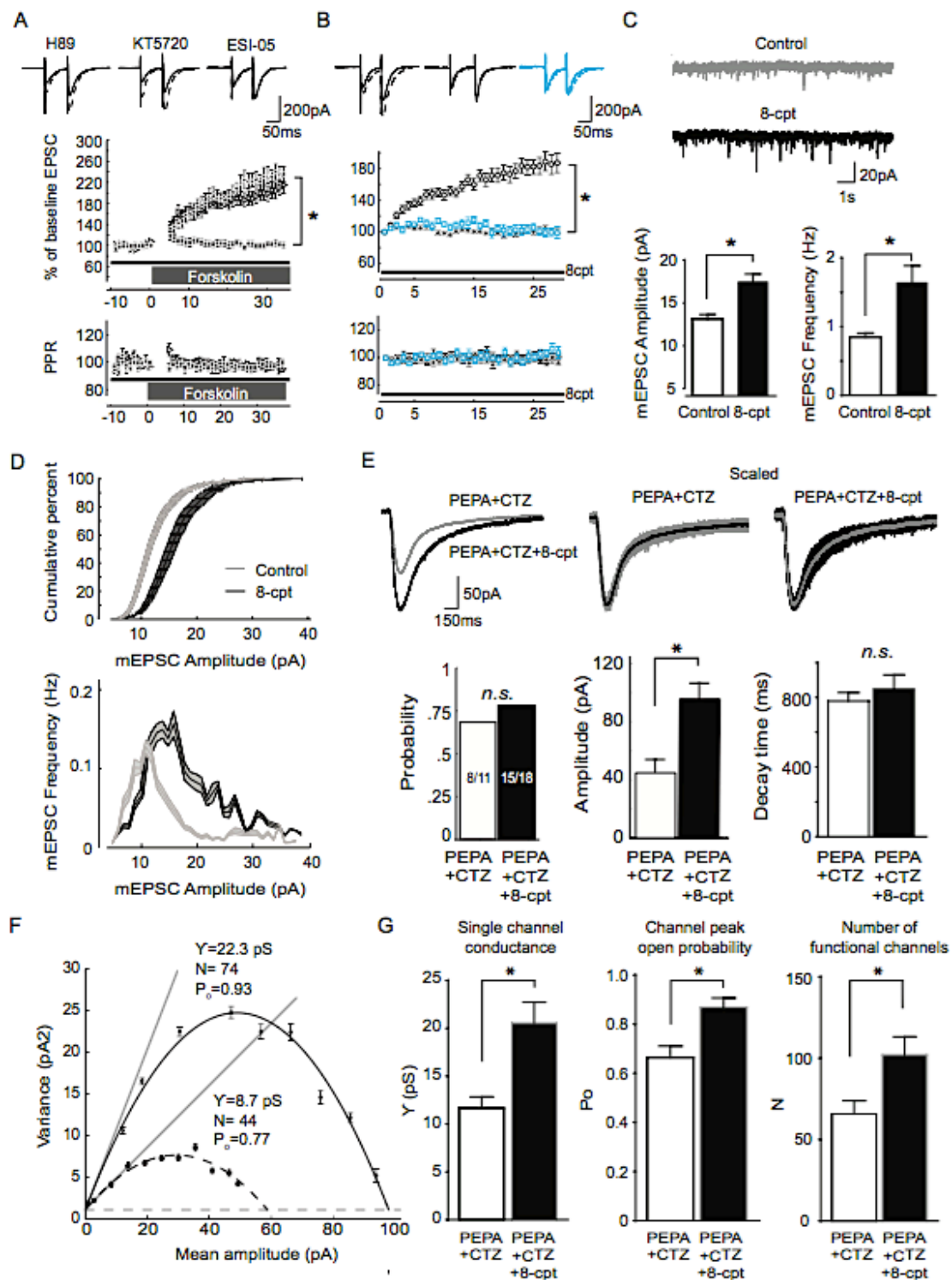


Figure 5. GluA3-plasticity requires cAMP-dependent postsynaptic activation of Epac.

(A) Epac2 antagonist ESI-05 blocks forskolin-driven synaptic potentiation, whereas PKA antagonists H89 and KT5720 do not. (B) Intracellular application of membrane-impermeable Epac agonist 8CPT caused significant synaptic potentiation in WT PCs (open circles) compared with GluA3-KO PCs (blue boxes) or no drug condition (closed circles). (C)

Intracellular application of 8CPT caused an increase in both mEPSC amplitude (left) and frequency (right). (D) A shift towards higher amplitudes was visualized both in the mEPSCs cumulative distribution and in the frequency versus amplitude distribution plots once again suggesting postsynaptic effects of EPAC activation. (E) Excised patches from PC somata generated significantly larger currents when 8CPT was present in the internal solution compared to control patches in the presence of AMPARs desensitization blockers (PEPA and CTZ). There were no differences in probability of having a patch presenting AMPA events or in event decay time kinetics. (F) Example parabolic distribution of the variance versus amplitude relationship obtained from bins of the current decay profile. Non-stationary noise analysis (NSNA) was done by fitting a parabolic equation to this distribution in order to estimate conductance, open probability and number of active receptors. (G) NSNA performed on the PC recordings in E revealed a significantly increased single channel conductance and peak open channel probability upon 8CPT application, which in turn led to an increased number of functional channels responding to the local AMPA application. Scale bars indicate 25 μm and 100 μm for cerebellar cortex and hippocampal images, respectively. Error bars indicate SEM, * indicates $p < 0.05$.

10 pA in response to puffs of 100 μM AMPA (Figure S6C). When the Epac activator 8CPT was added to the internal solution of the patch pipette, the peak current obtained under the same conditions was increased 2.5-fold in the absence of a presynaptic component (25 ± 3 pA, $p < 0.001$ vs. control). This difference in peak current was largely maintained in the presence of AMPAR desensitization blockers PEPA and cyclothiazide (45 ± 8 pA without vs. 97 ± 10 pA with 8CPT; $p < 0.001$, Figures 5G-H), indicating that cAMP-driven GluA3-plasticity does not involve a change in desensitization properties of AMPAR channels. As expected from our single channel results, non-stationary noise analysis of these non-desensitizing AMPAR responses showed a significant increase in conductance and open probability (Figures 5F-G). This approach revealed how in a mixed pool of GluA1- and GluA3-containing AMPARs Epac-dependent GluA3 potentiation was translated in an increase in current amplitude without altering the dynamics of the response (Figure 5E), highlighting the consistent results on the mEPSCs and eEPSCs.

Epac activation is required for LTP and motor learning

We next tested whether PF-PC LTP depends on Epac activation. Incubation of slices with Epac-inhibitor ESI-05 significantly inhibited synaptic potentiation induced by tetanic PF stimulation ($102 \pm 13\%$ versus $140 \pm 8\%$ in control conditions; $p < 0.0001$ after 15 min; Figure 6A). In addition, LTP was fully occluded when brain slices were pre-incubated with the membrane-permeable analog of Epac activator (8pCPT) (GluA3-KO vs. WT: $p = 0.008$; Figure 6B). Together, these data indicate that Epac2 activation

is responsible for postsynaptic LTP at the PF to PC synapse through activation of GluA3-containing AMPARs. To investigate the involvement of Epac activation in cerebellar synaptic plasticity *in vivo*, we performed phase reversal adaptation in WT mice that received daily IP injections with either Epac antagonist ESI-05 (0.2 - 0.3 ml

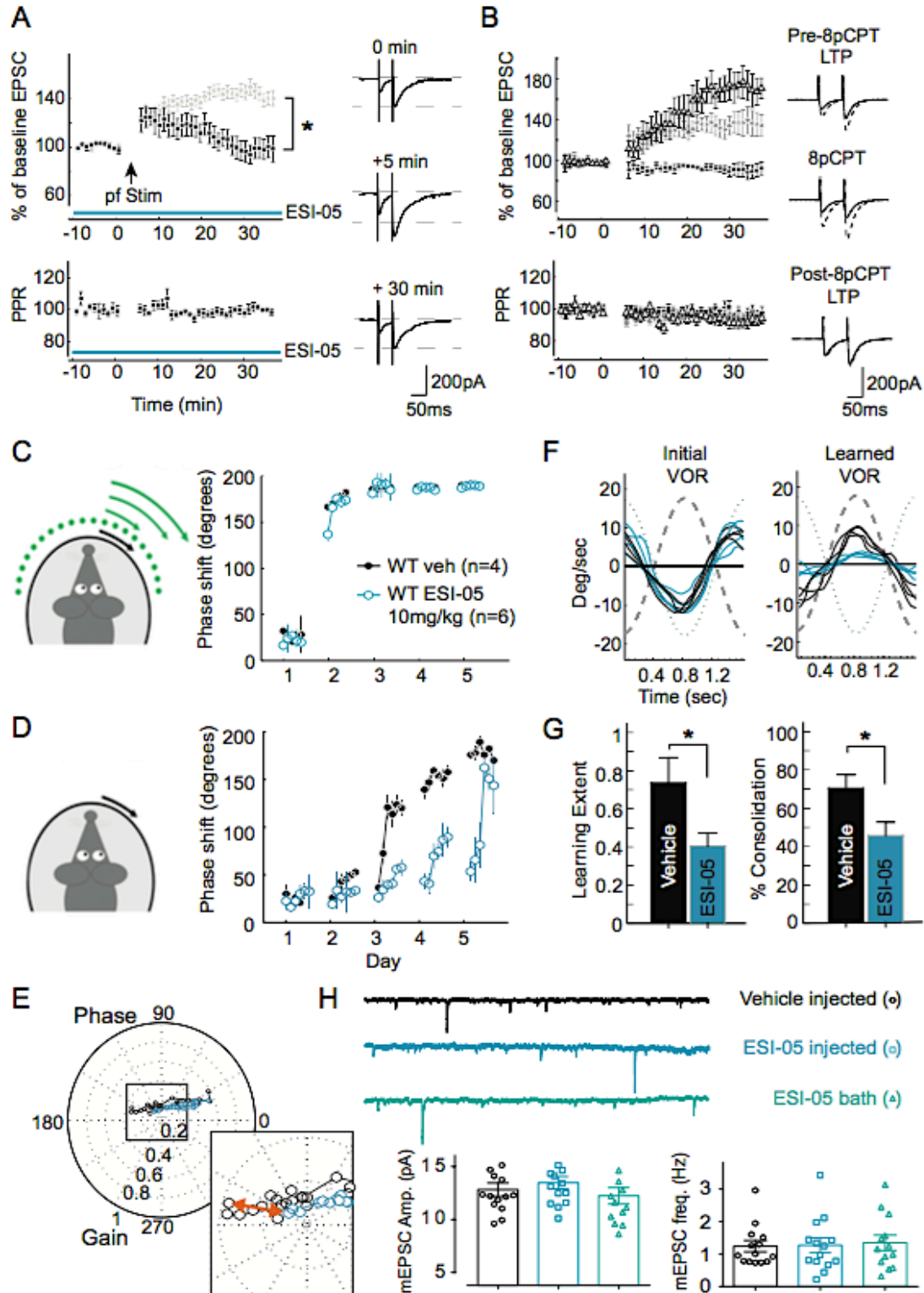


Figure 6. Pharmacological manipulation of Epac activity impairs LTP *in vitro* and motor learning *in vivo* without affecting synaptic transmission.

(A) Epac antagonist ESI-05 prevents PF to PC LTP induced by tetanic PF stimuli. (B) Long lasting Epac activation (minimum 30 minutes) produces synaptic potentiation that occludes LTP by saturating GluA3 dependent potentiation. (C) Eye movement phase values in wildtype mice injected with ESI-05 10 mg/kg (open blue circles) and injected with vehicle only (black circles) during visuo-vestibular mismatch training are virtually identical. (D) Phase values of VOR adaptation catch trials in mice injected with ESI-05 10 mg/kg show significantly impaired motor learning compared with those in their vehicle injected littermates, as observed by the significantly delayed reaching of the VOR phase reversal. (E) Polar plot of the gain and phase data combined with the data plotted in D shows a common learning trajectory and comparable initial gain for both groups. Inset: the final VOR reached after 5 days of training is amplified to visualize the magnitude of the gain difference between ESI-05 and vehicle injected mice. (F) Four representative eye velocity traces of the VOR before (left) and after (right) phase reversal training show that whereas both ESI-05 and vehicle injected mice show equal baseline performance and that both are able to flip the phase of the VOR. The magnitude of the VOR reached after the training is notoriously different. (G) Both learning extent and consolidation during the phase reversal task are significantly smaller in L7-GluA3 KO mice compared to those in WT littermates (T2-test $p < 0.05$). (H) Impaired motor learning after ESI-05 injections does not correlate with a decreased synaptic transmission. WT mice injected with ESI-05 show similar mEPSC amplitude and frequency to that in vehicle injected mice. ESI-05 did not modify mEPSC basal synaptic transmission either in non-injected mice when applied directly on the perfusion ACSF.

at 10 mg/kg) or with vehicle alone 30 minutes prior to the training protocol. Mice administrated with ESI-05 were not affected in basal eye reflex behavior, but performed significantly worse in the phase reversal task compared to vehicle injected animals (Figure 6D). Although both groups eventually reached a reversal of the VOR phase (Veh= $157 \pm 2\%$ and ESI-05= $148 \pm 15^\circ$, Figure 6D), its magnitude was significantly lower in the ESI-05 injected mice compared to vehicle controls ($p=0.01$; Figures 6E and F). This difference reached after training could not be explained by a poor basic response to the training stimuli (Figure 6C), but only by a significantly reduced learning extent ($p=0.01$) and consolidation rate ($p=0.03$). Importantly, systemic ESI-05 injections produced learning deficits without a change in basal synaptic transmission compared to vehicle-injected mice ($p=0.5$ and 0.9 for mEPSCs amplitude and frequency, respectively) (Figure 6H), suggesting that absence of Epac-dependent synaptic potentiation without any change in basal transmission is sufficient to impair learning capabilities.

GluA3 expression in Purkinje cells is required for VOR learning

We showed that VOR learning depends on global expression of GluA3 and that LTP at PF-PC synapses requires GluA3-plasticity, but does VOR learning depend on GluA3 specifically in PCs? To address this question, we generated and tested a PC-

specific GluA3-KO mouse (referred to as L7/GluA3-KO, Figure S9) by crossbreeding mice expressing Cre-recombinase under the PC-specific promoter L7-pcp2 with mice in which the GluA3 gene is flanked by loxP sites (Barski et al., 2000; Sanchis-Segura et al., 2006). After establishing the single-unit identity of floccular vertical-axis Purkinje cells in adult L7/GluA3-KO mice by demonstrating a climbing fiber pause in their simple spike activity as well as a preferred modulation tuning-curve during extracellular recordings in vivo (Figure S8A; see also Hoebeek et al., 2005), we investigated the baseline action potential generation of their simple spike activity in the awake state during spontaneous activity. Both the firing frequency and regularity (i.e. coefficient of variation of adjacent intervals of ISIs or CV2) of the simple spike activity of the L7/GluA3-KO mice did not differ significantly (both $p=0.8$) from those of wild types (Figure S8C), which is consistent with the I-V relationships recorded in vitro for GluA3-lacking PCs (Figure S8A). Next, we provided visual stimulation at the frequency that was used for the training paradigm (0.6 Hz). Again the firing frequency and regularity (i.e. CV2) of the simple spike activity of the L7/GluA3-KO mice did not differ from those of wild types ($p=0.7$ and $p=0.8$ respectively) (Figure 7A). Moreover and most importantly, the amplitude of the simple spike modulation during visual stimulation did not differ ($p=0.8$; Figure 7A). Finally, the firing frequency and modulation amplitude of the complex spikes did not show any significant difference either ($p=0.7$ and $p=0.9$, respectively; Figure 7A). Together, these data indicate that baseline excitability and spike generation of PCs in vivo is intact despite the reduced PF to PC synaptic transmission caused by the lack of GluA3 (Figure S8B).

We then subjected 3 to 5 months old L7/GluA3-KO and control littermates to the same behavioral tests as the global GluA3-KO. The baseline OKR and VOR performances of these L7/GluA3-KO mice were indistinguishable from those in controls (Figure S1). Similarly to global GluA3-KOs, VOR motor learning was prominently affected in L7-GluA3-KO mice (Figure 7C-G). The absence of GluA3 in PCs showed significant deficits throughout the whole phase-reversal paradigm (all p values <0.01 after day 2), including a significantly different learning extent at the end of it ($p<0.01$; Figures 7B, C and D). Moreover, consolidation during the phase-reversal paradigm as well as that during the gain-increase paradigm was significantly lower in L7/GluA3-KO compared to control littermates (both p values <0.01 ; Figures 7F and G). These data indicate that the behavioral phenotypes in motor learning observed in the global GluA3-KO can be largely attributed to a lack of GluA3-dependent synaptic plasticity in PCs.

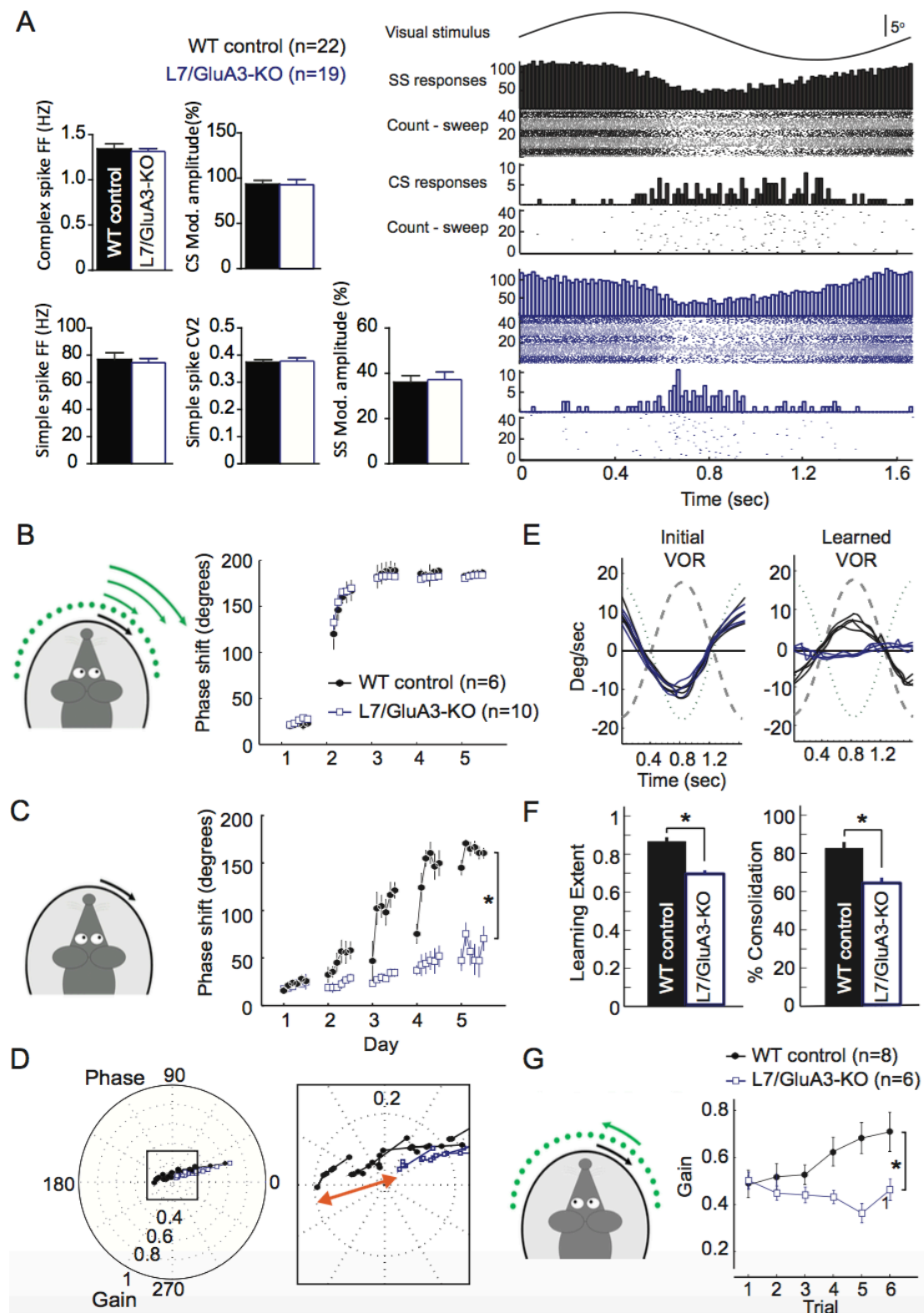


Figure 7. Lack of GluA3 in PCs causes motor learning deficits.

(A) Representative activity of vertical-axis Purkinje cells recorded in the flocculus of wild type and L7/GluA3-KO mice during visual stimulation (5° , 0.6 Hz). Bar graphs show that averages of frequency, CV2 and modulation amplitude of simple spikes, as well as frequency and modulation amplitude of complex spike during OKR stimulation were similar in control ($n = 22$) and L7/GluA3-KO mice ($n = 19$). The visual stimulus is shown together with histograms of

simple spike and complex spike frequencies and corresponding raster plots in the right panels. (B) Eye movement phase values in L7/GluA3-KO mice (open square) and WT mice (closed circle) during visuo-vestibular mismatch training are comparable. (C) Phase values of VOR adaptation catch trials in L7/GluA3-KOs show significantly impaired motor learning compared with those in their WT littermates. (D) Polar plot of the gain and phase data combined with the data plotted in B shows a common learning trajectory and comparable initial gain for both groups. Inset: the final VOR reached after 5 days of training is amplified to visualize the magnitude of the gain difference between L7/GluA3 KO and WT mice. (E) L7/GluA3-KOs (blue line) show equal baseline performance compared with WTs (black line), but are unable to reverse the phase of their VOR. Four representative eye velocity traces of the VOR before (left) and after (right) phase reversal training. (F) Both learning extent and consolidation during the phase reversal task are significantly smaller in L7-GluA3 KO mice compared to those in WT littermates (T2-test $p < 0.05$). (G) Gain-increase learning reveals deficits for L7/GluA3-KO compared to WT mice. Error bars indicate SEM, * indicates $p < 0.05$.

DISCUSSION

It is widely believed that LTP- and LTD-type synaptic plasticity mechanisms act in concert to mediate several types of learning in cerebral brain regions (Malinow and Malenka, 2002, Makino and Malinow, 2009; Nabavi et al., 2014; Nedelescu et al., 2010; Rumpel et al., 2005; Takahashi et al., 2003). For cerebellar learning LTD at PF to PC synapses has historically been considered the predominant plasticity mechanism (Ito, 2002; Linden and Connor, 1995). Although the simple spike suppression observed at early stages of some forms of motor learning in vivo may suggest LTD occurrence (Yang and Lisberger, 2014; ten Brinke et al., 2015), an increasing amount of studies suggest that LTD is not a strict requisite for motor learning (Hesslow et al., 2013; Schonewille et al., 2011). We present here the best evidence thus far that LTP at PF to PC synapses is a required mechanism for cerebellar motor learning. We show that LTP, but not LTD, at the PF to PC synapse requires plasticity of GluA3-containing AMPARs and that both the selective removal of GluA3 in PCs and the pharmacological blockade of the pathway leading to GluA3 plasticity in vivo severely impair the ability to adapt vestibulo-ocular reflexes. Combined, these findings provide the first correlative link between GluA3-dependent LTP and behavioral learning in general.

The possible role of LTP at the PF to PC synapse in cerebellar motor learning has been suggested before by two other cell-specific mouse mutant studies (Andreescu et al., 2007; Schonewille et al., 2010). However, these studies tackled central PC processes, which involved the nuclear estrogen receptor and cytosolic protein phosphatase calcineurin, and as a consequence they suffered from various side-effects downstream that prevented definitive conclusions (Gao et al., 2012). For example, application of estradiol also showed structural changes at the level of PC spines, while calcineurin turned out to be directly involved in induction of intrinsic plasticity through activation of SK-channels (Belmeguenai et al., 2010). In the current study, in which we tackled PF to PC LTP more downstream by targeting GluA3-containing AMPARs at the level of the synapse itself, we did not find any evidence for structural changes or firing differences in PCs of awake behaving mice. We did find that the basal transmission was reduced in PCs lacking GluA3 (both in the global and the cell specific KO mice), but this deficit was probably not the reason for the impairment of LTP and of motor learning, because acutely inhibiting GluA3-plasticity through blockade of Epac prevented both LTP and motor learning without affecting basal transmission. We therefore propose that the reduced basal transmission in GluA3-KO mice is the consequence of a prolonged deficit in LTP.

Synaptic potentiation through activation of GluA3-plasticity does not involve trafficking but rather an increase in open-channel probability of GluA3-containing receptors. This suggests that PF to PC LTP is mechanistically not just the reverse of LTD at this synapse (Jorntell and Hansel, 2006). Linden and colleagues have shown that PF to PC LTD is largely, but not exclusively, expressed by endocytosis of GluA2-containing AMPARs (Linden, 2001; Schonewille et al., 2011), thus mainly dependent on AMPAR trafficking. Given the current findings on GluA3-mediated LTP, it may be worthwhile to find out whether changes in AMPAR unitary conductance or glutamate affinity also play a minor role in early LTD expression at the PF to PC synapse, as interference with clathrin-mediated endocytosis produced a significant, but not total, attenuation of LTD expression (Wang and Linden, 2000).

The finding that an Epac-mediated change in single channel conductance and open probability of GluA2/3-containing AMPARs may underlie LTP at the PF to PC synapse raises the question how this change in configuration comes about. Interestingly, the distribution of GluA3-containing AMPARs openings does not seem to respond to a stochastic probability distribution of four ligand binding domains (LBDs) “catching” glutamate with equal probability. Instead it is biased towards the lowest conductance state opening, in which only two out of four LBDs bind glutamate. Because the formation of GluA3-homomers is energetically unfavorable (Sukumaran et al., 2011), most GluA3-containing AMPARs likely consist of two GluA3 and two GluA2 subunits. This might suggest that only the GluA2 LBDs effectively bind glutamate under basal conditions. Our observation that enhancing cAMP levels exerts GluA3-containing receptors to produce higher conductance openings (resembling the behavior of GluA1-containing receptors) may suggest that Epac activation triggers a conformational change in the two GluA3 subunits present in each tetramer, such that they become responsive to glutamate binding at the LBD (Figure 6F).

It is widely accepted that intracellular graded calcium signaling is a key mechanism for synaptic plasticity induction in PCs (van Woerden et al., 2009); small increases of Ca^{2+} concentration following PF stimulation can induce LTP, whereas high influxes of Ca^{2+} following climbing fiber activation can trigger LTD. In the present study we show that postsynaptic LTP depends on cAMP-dependent activation of GluA3-containing receptors. However, how low calcium signals in PCs are transduced into activation of adenylyl cyclase to raise cAMP levels remains to be elucidated. Interestingly, it has been shown that the tetanic activity of PFs required for LTP induction produces local calcium increases dependent on low threshold CaV3.1 T-type calcium channels

(Hildebrand et al., 2009) and that global deletion or blockage of these channels prevents LTP induction and motor learning (Ly et al., 2013). The calcium/calmodulin-dependent adenylyl cyclase *Adcy1* (Masada et al., 2012) could be an interesting candidate to convert local calcium activity in a rise in cAMP.

We here show that postsynaptic GluA3-dependent synaptic potentiation depends on a rise in cAMP. Therefore this study expands the repertoire of forms of PC plasticity already known to depend on cAMP, such as presynaptic plasticity (Chen and Regehr, 1997; Kaneko and Takahashi, 2004; Lev-Ram et al., 2002), intrinsic plasticity (Belmeguenai et al., 2010) or plasticity at inhibitory synapses (Mitoma and Konishi, 1996). *Epac2* has recently been reported to also have a role in presynaptic plasticity in that it may modify glutamate release probability (Gekel and Neher, 2008). This raises the interesting possibility that *Epac2* and/or cAMP in their pre- and postsynaptic domains operate in a synergistic fashion to control synaptic plasticity (Gao et al., 2012; Wang et al., 2014). Likewise, the induction protocol of LTP produces an increase in intrinsic excitability in PCs, via cAMP-mediated PKA modulation of SK potassium channels (Belmeguenai et al., 2010). Thus, since this change in intrinsic excitability occurs at least partly as a secondary process following tetanic PF stimulation, LTP at the PF to PC synapse may act as a feed-forward amplifier of synaptic inputs to modulate firing rate in PCs via cAMP production. Finally, it should be noted that rebound potentiation at the molecular layer interneuron to PC synapse, which occurs following PC depolarization, is also mediated by cAMP-mediated PKA modulation (Hirano and Kawaguchi, 2012). Together, these findings point towards a central role of cAMP following induction of PF to PC LTP, regulating multiple forms of plasticity with different identities and natures in a synergistic fashion (Gao et al., 2012).

In the present two manuscripts we highlight the role of GluA3-containing AMPARs in hippocampal and cerebellar plasticity. In both regions GluA3-mediated processes may operate under analogous rules at the cell biological level in that they both are cAMP-mediated and both do not entail activity-dependent synaptic trafficking. Yet, when we compare the functions of GluA3-containing AMPARs at the cell physiological and behavioral level with those of other AMPARs in the cerebellum and hippocampus, some striking differences emerge. First, whereas Renner et al. show that GluA3-mediated potentiation of hippocampal CA1-neurons does not directly affect contextual fear conditioning, we show here that GluA3-mediated LTP at the PF to PC synapse is required for cerebellar motor learning. Second, there is a striking difference with respect to the role of not only GluA3-containing AMPARs, but also

GluA1-containing AMPARs. Whereas the role of GluA3 in PC plasticity and cerebellar motor learning is now evident, that of GluA1 is still largely obscure. The presence of GluA1 in PCs was neither essential for the induction of LTD or LTP nor were there overt signs of deficits in motor performance or motor learning. Its possible role became only indirectly apparent, when we observed that, in contrast to the single GluA1-KO, the double GluA1/GluA3-KO virtually completely lacked glutamatergic currents in PCs. Possibly GluA1/2 heteromers in PCs serve to maintain basal synaptic currents when cAMP levels are low. Instead, the role of GluA1 in pyramidal cell function can hardly be overstated. GluA1-deficient mice display severe learning deficits not only in tasks that depend on the hippocampus, but also in those that rely on the amygdala or cortex (Humeau et al., 2007; Mead and Stephens, 2003). Taken together, the picture emerges that the learning rules for AMPAR-mediated plasticity in PCs are inverted compared with those in the hippocampus: cerebellar LTP and learning do not require GluA1, but depend on plasticity of GluA3-containing AMPARs, whereas hippocampal LTP and learning do not directly require GluA3, but depend on plasticity of GluA1-containing AMPARs.

REFERENCES

- Adamczyk,A., Mejias,R., Takamiya,K., Yocum,J., Krasnova,I.N., Calderon,J., Cadet,J.L., Huganir,R.L., Pletnikov,M.V., and Wang,T. (2012). GluA3-deficiency in mice is associated with increased social and aggressive behavior and elevated dopamine in striatum. *Behav. Brain Res.* 229, 265-272.
- Anzai,M., Kitazawa,H., and Nagao,S. (2010). Effects of reversible pharmacological shutdown of cerebellar flocculus on the memory of long-term horizontal vestibulo-ocular reflex adaptation in monkeys. *Neurosci. Res.* 68, 191-198.
- Barski, J.J., Dethleffsen, K., and Meyer, M. (2000). Cre recombinase expression in cerebellar Purkinje cells. *Genesis.* 28, 93-98.
- Bats, C., Farrant, M., and Cull-Candy, S.G. (2013). A role of TARPs in the expression and plasticity of calcium-permeable AMPARs: evidence from cerebellar neurons and glia. *Neuropharmacology* 74, 76-85.
- Belmeguenai, A., Hosy, E., Bengtsson, F., Pedroarena, C.M., Piochon, C., Teuling, E., He, Q., Ohtsuki, G., de Jeu, M.T., Elgersma, Y., De Zeeuw, C.I., Jorntell, H., and Hansel, C. (2010). Intrinsic plasticity complements long-term potentiation in parallel fiber input gain control in cerebellar Purkinje cells. *J. Neurosci.* 30, 13630-13643.
- Chen, C., and Regehr, W.G. (1997). The mechanism of cAMP-mediated enhancement at a cerebellar synapse. *J. Neurosci.* 17, 8687-8694.
- Douyard, J., Shen, L., Huganir, R.L., and Rubio, M.E. (2007). Differential neuronal and glial expression of GluR1 AMPA receptor subunit and the scaffolding proteins SAP97 and 4.1N during rat cerebellar development. *J. Comp Neurol.* 502, 141-156.
- Gao, Z., van Beugen, B.J., and De Zeeuw, C.I. (2012). Distributed synergistic plasticity and cerebellar learning. *Nat. Rev. Neurosci.* 13, 619-635.
- Gekel, I., and Neher, E. (2008). Application of an Epac activator enhances neurotransmitter release at excitatory central synapses. *J. Neurosci.* 28, 7991-8002.
- Gerlai, R., Henderson, J.T., Roder, J.C., and Jia, Z. (1998). Multiple behavioral anomalies in GluR2 mutant mice exhibiting enhanced LTP. *Behav. Brain Res.* 95, 37-45.
- Gutierrez-Castellanos, N., Winkelman, B.H., Tolosa-Rodriguez, L., De Gruijl, J.R., and De Zeeuw, C.I. (2013). Impact of aging on long-term ocular reflex adaptation. *Neurobiol. Aging* 34, 2784-2792.
- Hildebrand,M.E., Isope,P., Miyazaki,T., Nakaya,T., Garcia,E., Feltz,A., Schneider,T., Hescheler,J., Kano,M., Sakimura,K., Watanabe,M., Dieudonne,S., and Snutch,T.P. (2009). Functional coupling between mGluR1 and Cav3.1 T-type calcium channels contributes to parallel fiber-induced fast calcium signaling within Purkinje cell dendritic spines. *J. Neurosci.* 29, 9668-9682.
- Hirano, T., and Kawaguchi, S.Y. (2012). Regulation of inhibitory synaptic plasticity in a Purkinje neuron. *Cerebellum.* 11, 453-454.
- Humeau, Y., Reisel, D., Johnson, A.W., Borchardt, T., Jensen, V., Gebhardt, C., Bosch, V., Gass, P., Bannerman, D.M., Good, M.A., Hvalby, O., Sprengel, R., and Luthi, A. (2007). A pathway-specific function for different AMPA receptor subunits in

- amygdala long-term potentiation and fear conditioning. *J. Neurosci.* 27, 10947-10956.
- Ito, M. (2002). Historical review of the significance of the cerebellum and the role of Purkinje cells in motor learning. *Ann. N. Y. Acad. Sci.* 978, 273-288.
- Jorntell, H., and Hansel, C. (2006). Synaptic memories upside down: bidirectional plasticity at cerebellar parallel fiber-Purkinje cell synapses. *Neuron* 52, 227-238.
- Takegawa, W., and Yuzaki, M. (2005). A mechanism underlying AMPA receptor trafficking during cerebellar long-term potentiation. *Proc. Natl. Acad. Sci. U. S. A* 102, 17846-17851.
- Kaneko, M., and Takahashi, T. (2004). Presynaptic mechanism underlying cAMP-dependent synaptic potentiation. *J. Neurosci.* 24, 5202-5208.
- Kessels, H.W., and Malinow, R. (2009). Synaptic AMPA receptor plasticity and behavior. *Neuron* 61, 340-350.
- Lev-Ram, V., Wong, S.T., Storm, D.R., and Tsien, R.Y. (2002). A new form of cerebellar long-term potentiation is postsynaptic and depends on nitric oxide but not cAMP. *Proc. Natl. Acad. Sci. U. S. A* 99, 8389-8393.
- Linden, D.J. (2001). The expression of cerebellar LTD in culture is not associated with changes in AMPA-receptor kinetics, agonist affinity, or unitary conductance. *Proc. Natl. Acad. Sci. U. S. A* 98, 14066-14071.
- Linden, D.J., and Connor, J.A. (1995). Long-term synaptic depression. *Annu. Rev. Neurosci.* 18, 319-357.
- Makino, H., and Malinow, R. (2009). AMPA receptor incorporation into synapses during LTP: the role of lateral movement and exocytosis. *Neuron* 64, 381-390.
- Malinow, R., and Malenka, R.C. (2002). AMPA receptor trafficking and synaptic plasticity. *Annu. Rev. Neurosci.* 25, 103-126.
- Masada, N., Schaks, S., Jackson, S.E., Sinz, A., and Cooper, D.M. (2012). Distinct mechanisms of calmodulin binding and regulation of adenylyl cyclases 1 and 8. *Biochemistry* 51, 7917-7929.
- Mead, A.N., and Stephens, D.N. (2003). Selective disruption of stimulus-reward learning in glutamate receptor *gria1* knock-out mice. *J. Neurosci.* 23, 1041-1048.
- Meng, Y., Zhang, Y., and Jia, Z. (2003). Synaptic transmission and plasticity in the absence of AMPA glutamate receptor GluR2 and GluR3. *Neuron* 39, 163-176.
- Mitoma, H., and Konishi, S. (1996). Long-lasting facilitation of inhibitory transmission by monoaminergic and cAMP-dependent mechanism in rat cerebellar GABAergic synapses. *Neurosci. Lett.* 217, 141-144.
- Nedelescu, H., Kelso, C.M., Lazaro-Munoz, G., Purpura, M., Cain, C.K., Ledoux, J.E., and Aoki, C. (2010). Endogenous GluR1-containing AMPA receptors translocate to asymmetric synapses in the lateral amygdala during the early phase of fear memory formation. *J. Comp Neurol.* 518, 4723-4739.
- Nguyen-Vu, T.D., Kimpo, R.R., Rinaldi, J.M., Kohli, A., Zeng, H., Deisseroth, K., and Raymond, J.L. (2013). Cerebellar Purkinje cell activity drives motor learning. *Nat. Neurosci.* 16, 1734-1736.

Rumpel, S., Ledoux, J., Zador, A., and Malinow, R. (2005). Postsynaptic receptor trafficking underlying a form of associative learning. *Science* 308, 83-88.

Salin, P.A., Malenka, R.C., and Nicoll, R.A. (1996). Cyclic AMP mediates a presynaptic form of LTP at cerebellar parallel fiber synapses. *Neuron* 16, 797-803.

Sanchis-Segura, C., Borchardt, T., Vengeliene, V., Zghoul, T., Bachteler, D., Gass, P., Sprengel, R., and Spanagel, R. (2006). Involvement of the AMPA receptor GluR-C subunit in alcohol-seeking behavior and relapse. *J. Neurosci.* 26, 1231-1238.

Schonewille, M., Gao, Z., Boele, H.J., Veloz, M.F., Amerika, W.E., Simek, A.A., de Jeu, M.T., Steinberg, J.P., Takamiya, K., Hoebeek, F.E., Linden, D.J., Huganir, R.L., and De Zeeuw, C.I. (2011). Reevaluating the role of LTD in cerebellar motor learning. *Neuron* 70, 43-50.

Shi, S., Hayashi, Y., Esteban, J.A., and Malinow, R. (2001). Subunit-specific rules governing AMPA receptor trafficking to synapses in hippocampal pyramidal neurons. *Cell* 105, 331-343.

Sokolova, I.V., Lester, H.A., and Davidson, N. (2006). Postsynaptic mechanisms are essential for forskolin-induced potentiation of synaptic transmission. *J. Neurophysiol.* 95, 2570-2579.

Steinberg, J.P., Takamiya, K., Shen, Y., Xia, J., Rubio, M.E., Yu, S., Jin, W., Thomas, G.M., Linden, D.J., and Huganir, R.L. (2006). Targeted in vivo mutations of the AMPA receptor subunit GluR2 and its interacting protein PICK1 eliminate cerebellar long-term depression. *Neuron* 49, 845-860.

Sukumaran, M., Rossmann, M., Shrivastava, I., Dutta, A., Bahar, I., and Greger, I.H. (2011). Dynamics and allosteric potential of the AMPA receptor N-terminal domain. *EMBO J.* 30, 972-982.

Takahashi, T., Svoboda, K., and Malinow, R. (2003). Experience strengthening transmission by driving AMPA receptors into synapses. *Science* 299, 1585-1588.

Tsalkova, T., Mei, F.C., Li, S., Chepurny, O.G., Leech, C.A., Liu, T., Holz, G.G., Woods, V.L., Jr., and Cheng, X. (2012). Isoform-specific antagonists of exchange proteins directly activated by cAMP. *Proc. Natl. Acad. Sci. U. S. A* 109, 18613-18618.

Ten Brinke MM, Boele HJ, Spanke JK, Potters JW, Kornysheva K, Wulff P, Ijpelaar AC, Koekkoek SK, De Zeeuw CI. (2015) Evolving Models of Pavlovian Conditioning: Cerebellar Cortical Dynamics in Awake Behaving Mice. *Cell Rep.* 13(9), 1977-88.

van Woerden, G.M., Hoebeek, F.E., Gao, Z., Nagaraja, R.Y., Hoogenraad, C.C., Kushner, S.A., Hansel, C., De Zeeuw, C.I., and Elgersma, Y. (2009). betaCaMKII controls the direction of plasticity at parallel fiber-Purkinje cell synapses. *Nat. Neurosci.* 12, 823-825.

Wang, D.J., Su, L.D., Wang, Y.N., Yang, D., Sun, C.L., Zhou, L., Wang, X.X., and Shen, Y. (2014). Long-term potentiation at cerebellar parallel fiber-Purkinje cell synapses requires presynaptic and postsynaptic signaling cascades. *J. Neurosci.* 34, 2355-2364.

Wang, Y.T., and Linden, D.J. (2000). Expression of cerebellar long-term depression requires postsynaptic clathrin-mediated endocytosis. *Neuron* 25, 635-647.

Woolfrey, K.M., Srivastava, D.P., Photowala, H., Yamashita, M., Barbolina, M.V., Cahill, M.E., Xie, Z., Jones, K.A., Quilliam, L.A., Prakriya, M., and Penzes, P. (2009). Epac2 induces synapse remodeling and depression and its disease-associated forms alter spines. *Nat. Neurosci.* *12*, 1275-1284.

SUPPLEMENTARY FIGURES

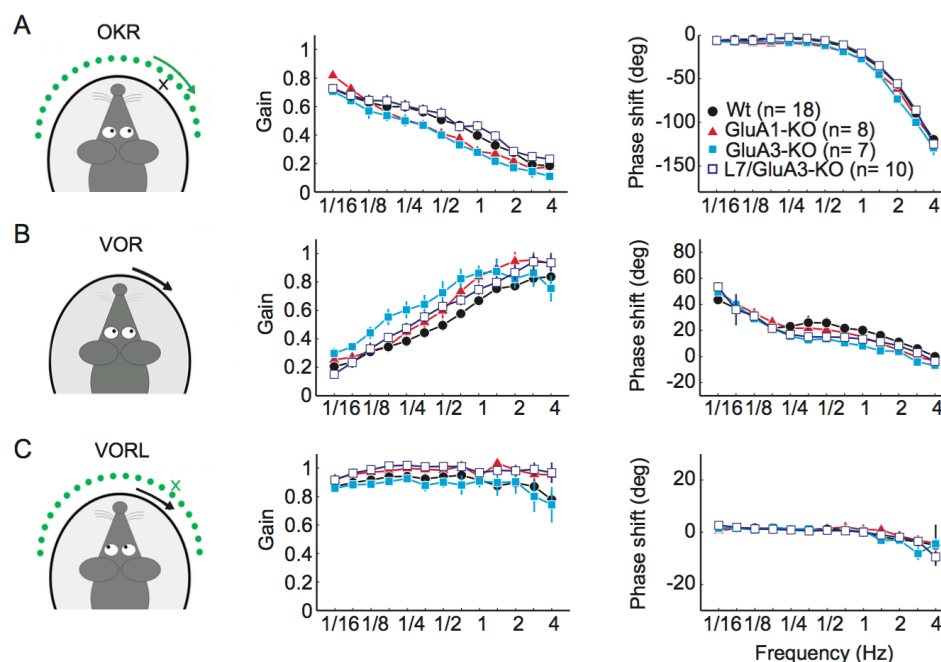


Figure S1. Basic compensatory eye movements are largely unaffected in global KO mice for GluA1 or GluA3 as well as in PC-specific KO for GluA3. (A) The optokinetic reflex (OKR), which stabilizes gaze with respect to a moving visual field (Stahl et al., 2000), showed a normal baseline gain in GluA1-KO and GluA3-KO mice ($F(2,29)=2361$, $p = 0.11$; Repeated measures ANOVA and Tukey Post-Hoc analysis), whereas phase values in both mutants presented a small, but consistent, delay across the entire frequency range tested ($F(2,29)=14.86$, $p < 0.01$, Tukey's multiple comparisons test revealed differences for the 95% confidence intervals of both mutants with respect to wild-type controls, but not between them). In contrast, L7/GluA3-KO mice presented intact gain and phase values compared to controls ($F(1,26) = 0.21$, $p = 0.64$ and $F(1,26) = 1.24$, $p = 0.27$, respectively). (B) During VOR compensation GluA1-KO and GluA3-KO showed both a normal gain ($F(2,29)=1745$, $p = 0.17$) and normal phase ($F(2,29)=1382$, $p = 0.26$). In addition, L7/GluA3-KO mice also showed a normal basic eye movement performance ($F(1,26) = 1.65$, $p = 0.21$ and $F(1,26) = 1.53$, $p = 0.22$, for gain and phase, respectively). (C) Finally, when we combined optokinetic stimulation with vestibular stimulation (i.e. VOR in the light or VORL) as occurs in daily life, all mutants also showed normal performances for both gain and phase compared to those in wild-type littermates (i.e. $F(1,26) = 1.51$, $p = 0.23$ for L7/GluA3-KO vs. control gain values).

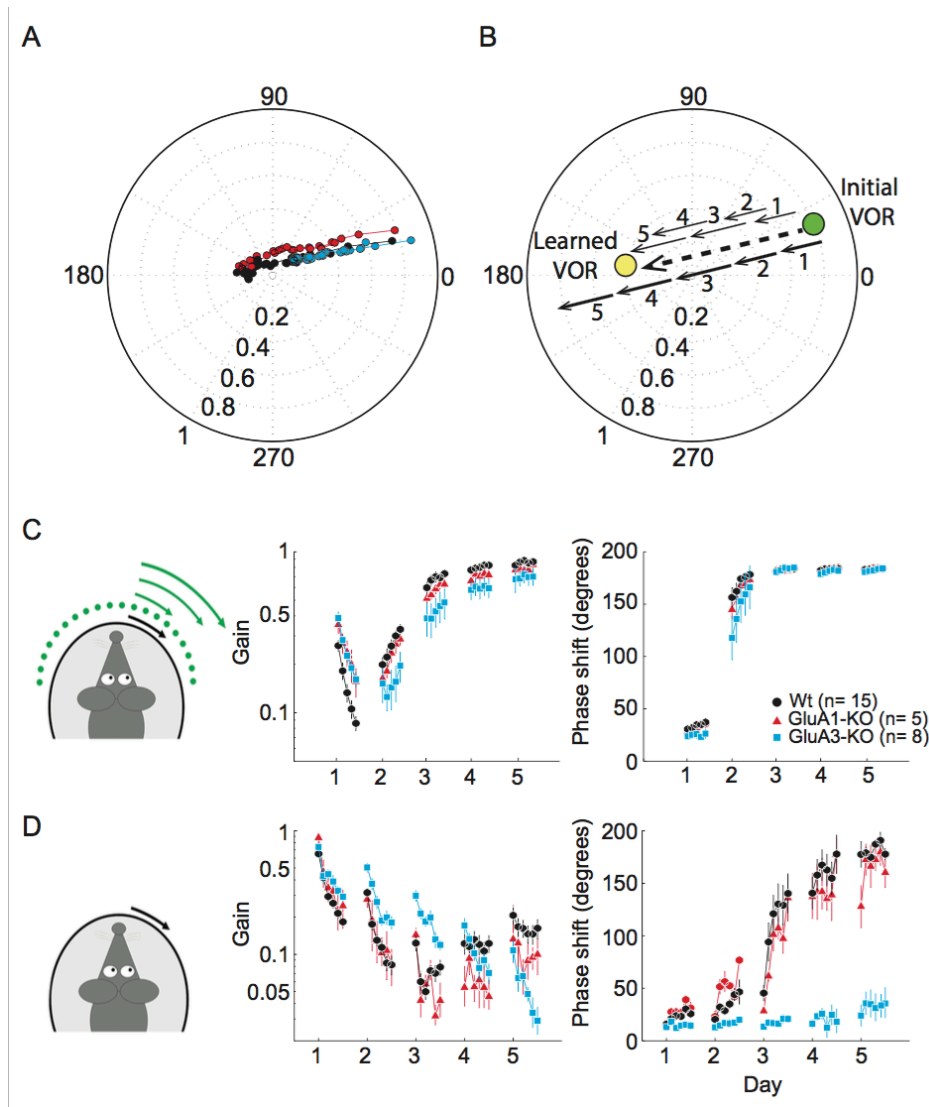


Figure S2. (A) The full range of the 2 variables that explain ocular movements (0 to 1 for the gain and 0 to 360 for the phase) determine a circular bi-dimensional Cartesian plane (shown as a polar plot) in which every eye movement can be defined. Given that phase-reversal learning takes place through a defined common learning trajectory (left polar plot) over several days during which phase covariates with gain, we performed statistics on the Cartesian coordinates defining gain and phase using the paired Hotelling's T2-Test. (B) Polar plots of gain and phase vectorial representation during phase reversal VOR learning data to illustrate the data analysis procedure. The data are composed of 5 individual learning vectors (one per day) moving across a constant learning trajectory towards the target set by the training paradigm (Phase, 180 degrees; Gain, 1). Based on the raw gain and phase data (A), we first calculate the Learning extent for each mouse as the vectorial difference between the final performance and the initial performance (recording 6 of day 5 – recording 1 of day 1) and subsequently average these values per group. Between days of training there is partial retention of motor memories; to calculate the overall consolidation we calculate the ratio between the learning extent and the absolute summed extent of the learning vectors as if there was no memory loss overnight (100% consolidation). This ratio calculated per mouse is then also averaged across the mice composing consolidation values for each group. (C) Behavior of 4-6 week old GluA3-KO mice shows phenotype that is virtually identical to that of 3-5 month old mice. Scatter plots of gain and phase values of 4-6 week old mice during the visuo-vestibular training for VOR phase reversal shows no significant differences in the ability to follow the training signal ($p > 0.05$ for last training recording on day 5 comparisons GluA1-

KO vs GluA3-KO and WT vs GluA3-KO). (D) Scatter plots of gain and phase values of the VOR catch trials show that WT and GluA1-KO mice, but not GluA3-KO mice, are able to reverse the phase of the VOR after training ($p < 0.01$ for last catch recording on day 5 comparisons GluA1-KO vs GluA3-KO and WT vs GluA3-KO). For comparison with data in 3-5 month old animals see also Figure 1.

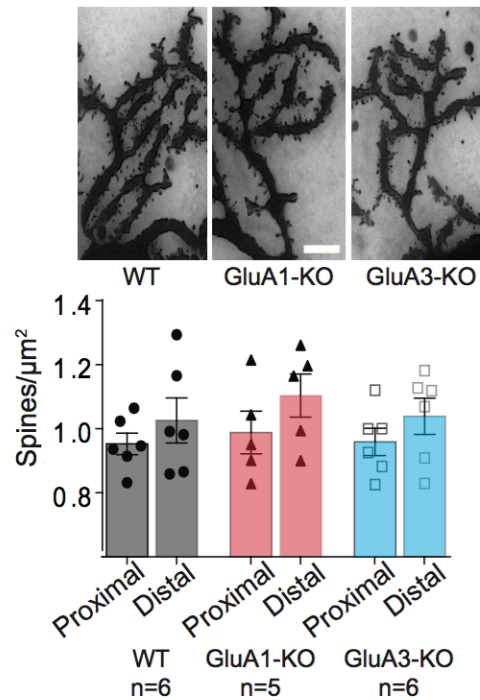


Figure S3. PCs lacking GluA1 or GluA3 have comparable spine density that is comparable to that in wild type (WT) PCs. Top panels show representative pictures of PC dendrites labeled with Golgi silver impregnation used to quantify spine densities of WT, GluA1-KO or GluA3-KO PCs. The results show that neither the lack of GluA1 nor that of GluA3 yielded differences in spine densities of proximal or distal dendrites of PCs (bottom panel). Densities plotted correspond to the average spine density of at least 20 dendritic branches of PCs located in lobules V to X per animal used for each genotype. Scale bar = 5 μm .

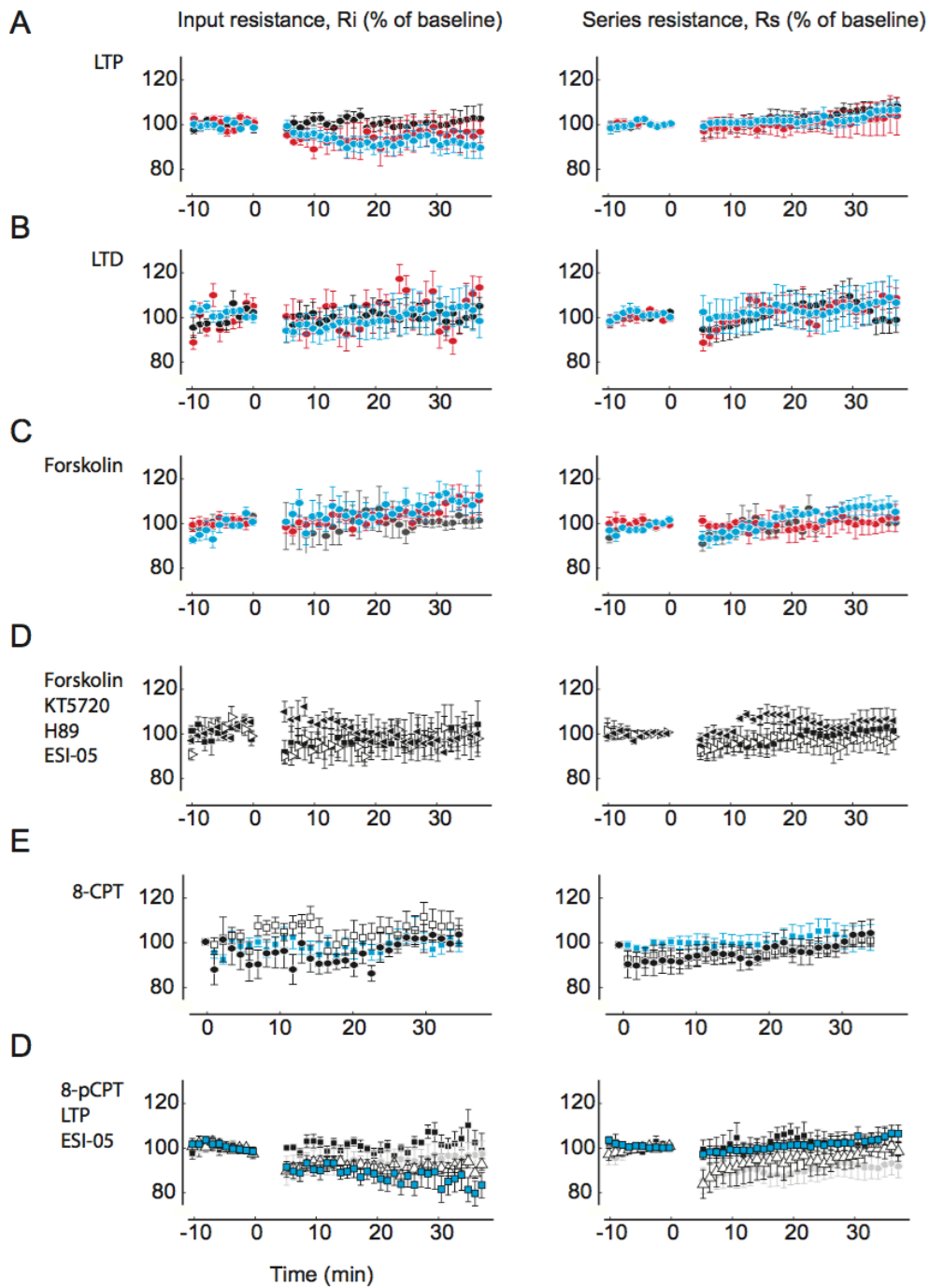


Figure S4. Overview of membrane resistance (R_m) and series resistance (R_s) of every group of PCs used to generate the experimental figures of the current study. Data are plotted with the same color code as in main figures. All PCs that had a change in resistance bigger than 20% over a period longer than 2 minutes were discarded for further analysis.

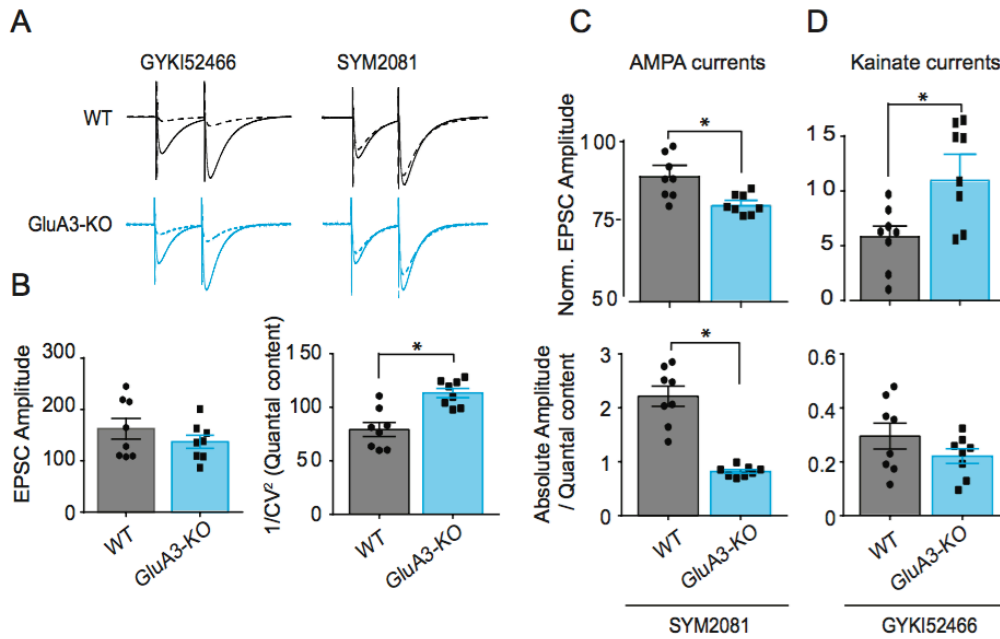


Figure S5. Kainate receptors do not compensate for weakening of glutamatergic transmission at PF to PC synapses in the absence of GluA3. (A) To assess possible compensatory components in the glutamatergic transmission of PCs in GluA3-KO mice we investigated the impact of blocking either AMPA-receptors with 30 μ M of GYKI-52466 (Cossart et al., 2002) or kainate receptors with 5 μ M of SYM2081 (Yan et al., 2013) after establishing a stable baseline of eEPSCs in WT and GluA3-KO PCs. (B) PF stimulation intensity was manually adjusted to obtain comparable EPSC amplitudes between 100-200 pA in WT and GluA3-KO PCs ($p=0.3$, GluA3-KO vs. WT). The average quantal content released to produce events of comparable amplitude (estimated as the inverse of the square coefficient of variation; (Kerchner and Nicoll, 2008), was significantly higher in the GluA3-KO ($p < 0.001$), indicating post-synaptic weakening. (C) Blocking AMPARs reduced the total glutamatergic transmission in GluA3-KO PCs by $89\pm 2\%$, which was significantly less than that in wild-type PCs ($94\pm 2\%$; $p = 0.01$ for GluA3-KO vs. WT, top panel). However, this difference was exacerbated after normalizing the amplitude to the quantal content, revealing that in the absence of GluA3, PCs have about half the normal magnitude of AMPA-mediated current ($p < 0.001$, bottom panel). (D) To investigate to what extent kainate receptors can compensate for an impairment in GluA3-dependent transmission in PCs (Yan et al., 2013), we investigated the impact of a blockage of kainate-receptors in both WT and GluA3-KO PCs. The contribution of kainate-receptor mediated events to EPSC amplitude normalized to baseline magnitude was significantly higher in PCs of GluA3-KO ($21\pm 1.5\%$) than that in WT PCs ($16\pm 3\%$; $p = 0.024$ for GluA3-KO vs. WT, top panel). However, when normalized to the quantal content, the absolute contribution of kainate receptors is comparable among genotypes ($p=0.19$, bottom panel). Together, these data indicate that glutamatergic transmission in GluA3-KO mice can be largely explained by GluA1/GluA2-mediated AMPA-currents and to a lesser extent by kainate-currents, none of which is able to compensate for the synaptic weakening caused by the absence of GluA3.

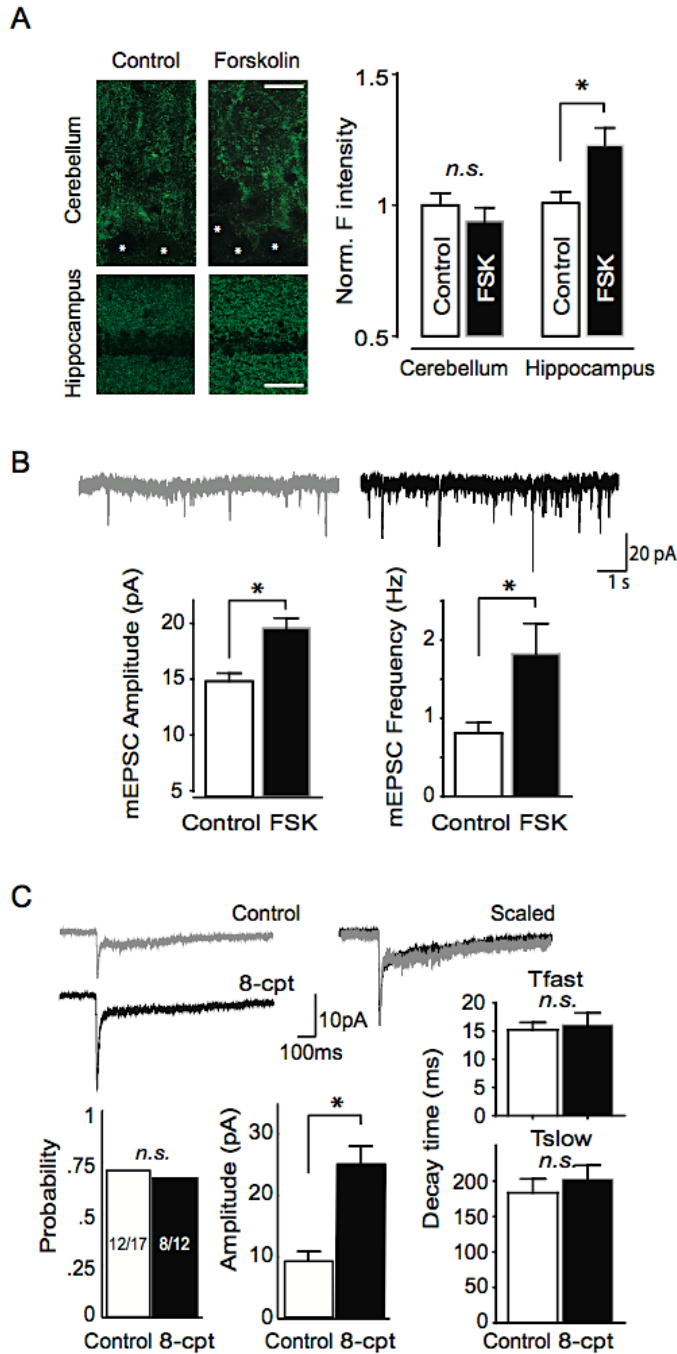


Figure S6. (A) Fluorescence intensity quantified in confocal images of the cerebellum after surface immunodetection for GluA2 subunits in slices of WT mice perfused with ACSF containing 50 μ M forskolin (Fsk) and normalized to control immunostaining intensity (extracellular domain of Nav1.2/SCN2A) revealed no differences in surface levels of AMPARs compared to those obtained from WT mice perfused with ACSF without Fsk ($p = 0.44$). However, in the hippocampus, sections of the same brains processed in the same runs did reveal a significant increase after Fsk application ($p = 0.035$). (B) Both amplitude and frequency of mEPSCs were significantly increased following the exact same ACSF + 50 μ M FSK perfusion used for A. Control data are also obtained as in A. (C) Excised patches from PCs somata that received puffs of 100 μ M AMPA generated significantly larger currents when 8-CPT-2Me-cAMP (8-CPT) was present in the internal solution compared to control patches

with the same probability of having a patch presenting AMPA events. Fast desensitizing and slow decay time kinetics were also unchanged.

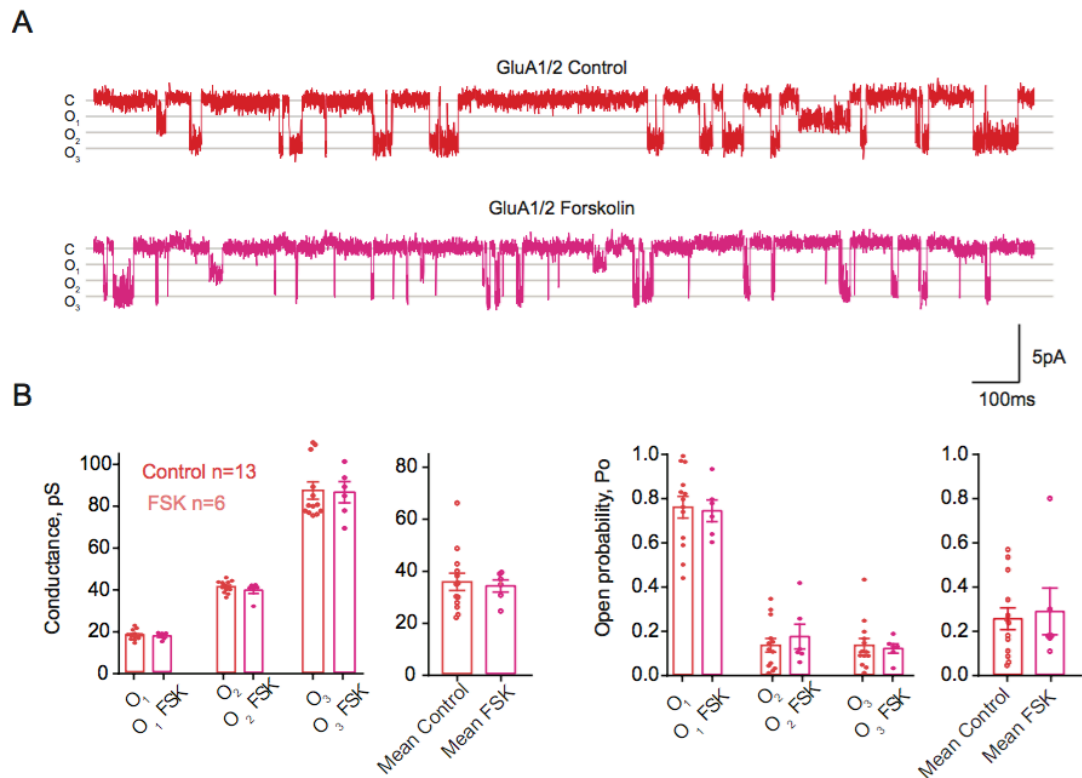


Figure S7. GluA1-containing AMPARs single channel properties are unchanged after forskolin application. (A) Example multichannel activity recording. The presence of “escalated” openings that produced multiple conductance levels before reaching baseline was the criterion used to discard recordings with multiple channels. (B) Representative traces of cell attached single channel recordings of GluA2/3 AMPARs in PCs of GluA1-KO mice. GluA1-containing AMPAR single channel activity in the presence and absence of forskolin show comparable behavior, with a clearly higher conductance level than GluA3 channels on basal conditions as shown in main Figure 4. (C) Conductance of the 3 different open levels of these channels is unchanged in the presence of forskolin and also comparable to that of GluA3 channels. (D) In addition, the relative fraction of openings and overall open probability of GluA1 channels was also unchanged after forskolin application and it resembles that of cAMP activated GluA3 channels.

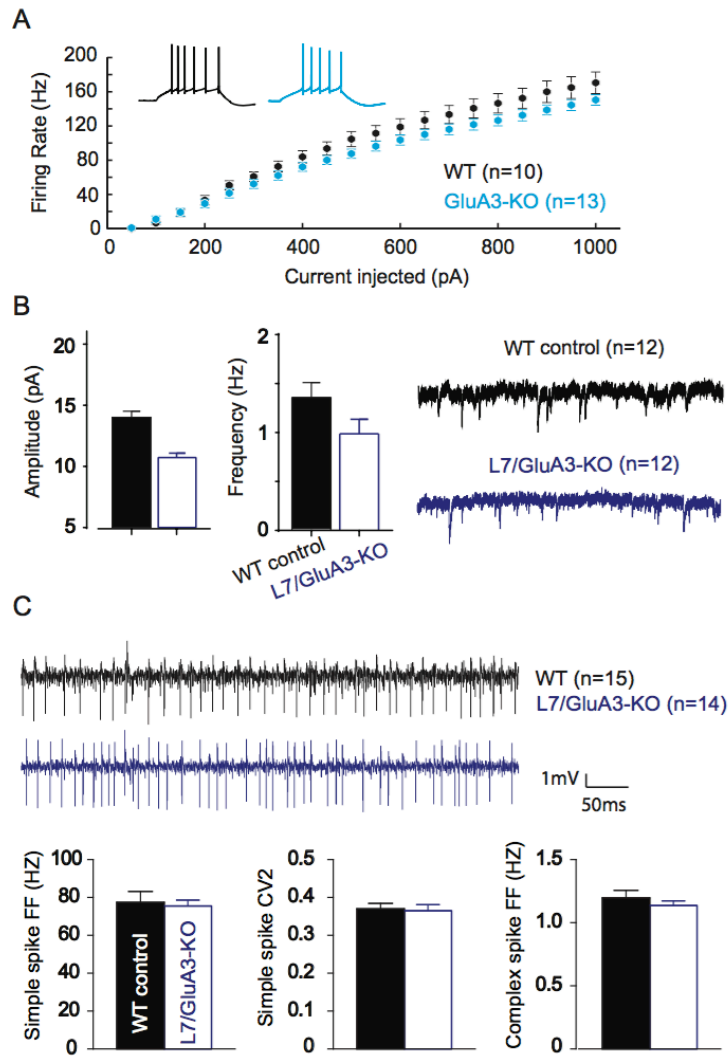


Figure S8. GluA3 lacking PCs show intact excitability in vitro and in vivo despite their reduced synaptic transmission. (A) Short square steps of increasing current injected into PCs of both wild-types and GluA3-KOs showed no differences in the I/V relationships between genotypes ($F(1,21)=2.3$, $p = 0.14$, Repeated Measures ANOVA), showing that despite the weaker synaptic transmission in the absence of GluA3, PCs have unchanged excitability in vitro. (B) Synaptic transmission is also reduced in the PC specific KO for GluA3 (L7/ GluA3-KO) tested in vitro. (C) In vivo spontaneous firing of L7/ GluA3-KO PCs show comparable firing frequency and regularity of simple spikes as well as comparable amount of complex spikes suggesting once more, that despite lower PF to PC synapses, PC excitability is unaffected.

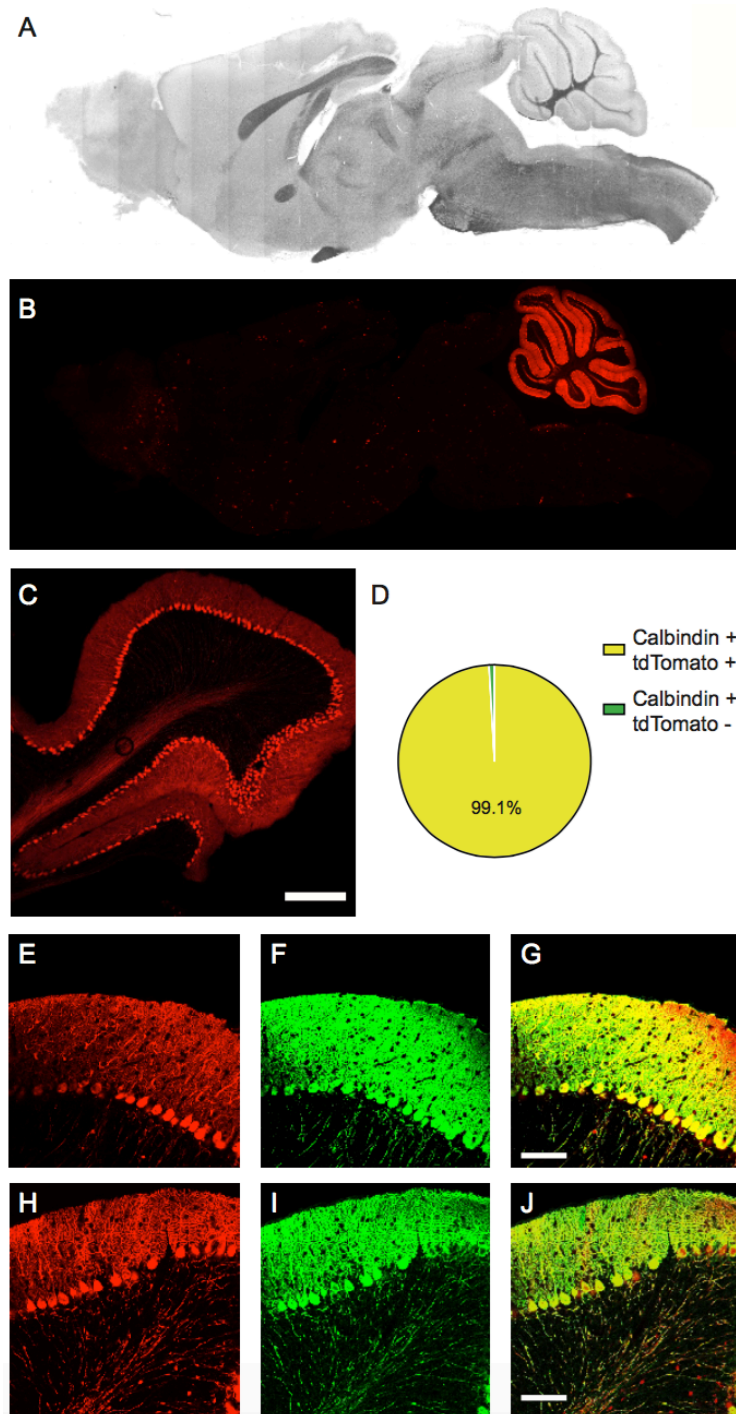


Figure S9. Cre dependent tdTomato expression under the L7 promoter confirms its Purkinje cells specificity. (A) Example view of a L7Cre/floxedGluA3-KO mouse sagittal brain slice in bright field. (B) Same brain slice imaged with an epifluorescence microscope reveals how tdTomato expression is restricted to cerebellar PCs. (C) PCs in the vestibulocerebellum (flocculus and paraflocculus) also express the reporter under the L7 promoter. (D) Quantification of the population of PCs expressing tdTomato under the L7 promoter (E, H) out of the total PC population detected by Calbindin immunohistochemistry (F,I) reveals that nearly all PCs are double labeled (G,J) proving that the L7 promoter can effectively be used to genetically manipulate virtually the entire population of PCs.

EXPERIMENTAL PROCEDURES

Mice

Inbred breeding colonies were used to obtain the experimental knockout mice. GluA1-KO mice, kindly provided by Dr. R. Huganir (Kim et al., 2005), were generated by mating heterozygous c57bl6/129 mice; GluA3-KO and wild-type littermates were bred from c57bl6x129P2-Gria3tm1Dgen/Mmnc mutant ancestors (MMRRC, Davis, CA) at least 6 times backcrossed to c57bl6 mice; and Purkinje cell specific GluA3 knockout mice were generated by crossing floxed GluA3 mice (Sanchis-Segura et al., 2006) with L7-Cre mice (Barski et al., 2000). All experiments were conducted in line with the European guidelines for care and use of laboratory animals (Council Directive 86/609/EEC). The experimental protocol was approved by the Animal Experiment Committee (DEC) of the Royal Netherlands Academy of Arts and Sciences (KNAW).

Eye movement recordings and oculomotor learning tasks

Baseline performance of compensatory eye movements and VOR adaptation were first tested in three groups of male mice at the age of 4-6 weeks and 3-5 months. These included wild-type littermate mice (WT, $n = 15 + 14$, for both age categories, respectively), GluA1 knockout mice ($n = 5 + 6$) and GluA3 knockout mice ($n = 8 + 6$). Mice were surgically prepared for chronic head restrained experiments (de Jeu and De Zeeuw, 2012). During the experiment the mouse was placed head-fixed in a holder tube on a vestibular motion platform (R2000 'Rotopod', Parallel Robotic Systems Corporation, Hampton, USA). Left eye orientation was measured using video pupil tracking with a table-fixed CCD camera (Pulnix TM-6710CL, 120 frames/s) and IR illumination (850 nm LED, 6.5 cm distance from the eye). Pilocarpine (2%) eye drops were applied before the experiment to limit pupil dilatation in darkness. Online image analysis was performed to extract the location of pupil edges and corneal light reflections using custom built software for Labview (National Instruments, Austin, TX, USA). Angular eye velocity was computed offline using custom software written for Matlab (The Mathworks Inc., Natick, MA) using the algorithm outlined elsewhere (Stahl et al., 2000). Saccadic eye movements and quick-phases of the vestibular nystagmus were removed using a $50^\circ/s$ velocity threshold and 200 ms margins at each threshold crossing. Each mouse was accustomed to the setup for a period of three training days before the experimental data was collected. The horizontal VOR was characterized in both darkness and light using sinusoidal rotation about the vertical axis, using frequencies ranging between

1/16th to 4 Hz, presented in a sequence of increasing order, holding constant peak velocity of 18.8°/s. The number of cycles ranged between 5 at 1/16Hz to 60 at 4 Hz. Mice were subjected to a VOR cancellation stimulus on the first day (in-phase sinusoidal movement at 0.6 Hz, 5° amplitude of both the table and the visual surround) and a VOR reversal stimulus on subsequent days (2-5), where the amplitude of the visual surround was increased to 7.5° (day 2) and 10° (days 3, 4, and 5). The amplitude of the turntable remained constant at 5° amplitude (18.8°/s peak velocity). Training sessions consisted of 6 VOR measurements (30 cycles, 50 seconds, in darkness) that were alternated with 5 periods of visuo-vestibular mismatch training (300 cycles, 500 seconds). Apart from the training sessions, animals were kept in total darkness during the consecutive training days. The eye movement response was expressed as gain and phase shift relative to head movement, which was calculated using multiple linear regression of eye velocity to in-phase and quadrature components of the turntable velocity trace. Gain of the eye movement response was defined as the ratio between the eye velocity and the table velocity magnitudes. Phase shift was expressed in degrees and offset by 180°, so that a phase of 0° indicates an eye movement that is in-phase with contraversive head movement; positive phase shift indicates phase lead. Consolidation of the adapted VOR was assessed by computing the ratio between the long-term change in VOR and the cumulative sum of short-term changes in VOR of preceding training sessions. The long-term change was defined as the absolute difference between the ending VOR on day 5 and the naive VOR on day 1. The short-term change was defined as the absolute difference between the VOR at the end of a training session and the beginning of a training session. For a period of at least 10 days animals were allowed to rest between different VOR adaptation protocols. Bivariate 2-sample Hotelling's T2-test was used to compare gain and phase values between groups, and One Way ANOVA/ Tukey post-hoc test was used for cumulative consolidation values.

Spine density quantification in Purkinje neurons

A commercially available kit (FD Rapid GolgiStain, FD Neurotechnologies, Inc., Columbia, USA) was used to perform the Golgi silver impregnation that was employed to calculate the spine density in PCs of WT (n=6) and KO mice (GluA1 n=5 and GluA3 n=6). Thick histological sections (100-150 µm) were obtained with a freezing microtome (Thermo Fisher Scientific, Waltham, MA, USA), dehydrated, permanently mounted with Permount (Thermo Fisher Scientific, Waltham, MA, USA) and imaged with a XYZ axis motorized control brightfield microscope (Zeiss Axioskop

9811 - Sony XC77 black and white video camera). Stacks of pictures across the Z-axis (10-30 μm) were made to count total spine number in proximal (max 30 μm away from the PC soma) and distal dendrites of PCs. The spine density was calculated for each dendrite dividing the dendrite's spine count by its length; all images were processed using ImageJ. All proximal and distal dendrites counted were averaged for each mouse and mice of the same genotype were averaged to obtain the final spine densities (Figure S5).

In Vitro Electrophysiology

Sagittal slices of the cerebellar vermis (250 to 400 μm thick) from 4 to 6 weeks old mice were obtained in ice-cold oxygenated "slicing" solution containing (in mM) 2.5 KCl, 1 CaCl₂, 3 MgCl₂, 25 NaHCO₃, 1.25 NaH₂PO₄, 240 sucrose, 25 D-glucose and 0.01 kynurenic acid. Slices were transferred to the same slicing solution at 34°C for 5-10 minutes and then transferred to oxygenated ACSF at 34°C containing (in mM) 124 NaCl, 5 KCl, 1.25 Na₂HPO₄, 1 MgSO₄, 2 CaCl₂, 26 NaHCO₃, 20 D-glucose. Subsequently, the slices were allowed to recover for at least 30 minutes until they were moved to the recording chamber containing the same oxygenated ACSF with 100 μM picrotoxin to prevent GABAergic transmission at near physiological temperature of 30 \pm 2°C. Whole-cell patch-clamp recordings of Purkinje cells located in lobules VI to X were performed using an EPC-10 amplifier (HEKA, Lambrecht). 3-5 M Ω resistance patch pipettes were filled with (in mM) K-Gluconate 122.5 mM, NaATP 4, NaGTP 0.4, HEPES 10, NaCl, KCl 9 and 0.6 mM EGTA (Sigma) at pH 7.25 for all the recordings that required current clamp mode (including LTP) or with (in mM) 115 mM cesium methanesulfonate, 20 mM CsCl, 10 mM HEPES, 2.5 mM MgCl₂, 4 mM Na₂ATP, 0.4 mM Na₃GTP, 10 mM sodium phosphocreatine (Sigma), and 0.6 mM EGTA (Sigma), at pH 7.25 for the experiments that were exclusively done in voltage clamp mode. For both voltage-clamp and current-clamp recordings, PC membrane potential was held at -70mV to prevent spontaneous firing. Series resistance (5-10 M Ω) was measured before the experiment and compensated with standard procedures. During the experiment series and membrane resistances were monitored by applying a 100 ms hyperpolarizing pulse (-10 mV). Only cells with stable membrane and series resistance (change < 20% of the last 5 minutes of recordings compared to the last 5 minutes of baseline, figure S4) were included in the analysis. Whole-cell recordings were digitized at 40 kHz and filtered with a Bessel filter at 4 kHz for voltage clamp recordings (8 kHz for current clamp mode). PF to PC LTD was induced by pairing PF stimulation at 1Hz for 1 minute with a 100 ms somatic depolarization from 70 mV to 0

mV, mimicking climbing fiber input (Linden, 2001; Saab et al., 2012). Instead, PF to PC LTP was induced by PF stimulation alone at 1 Hz for 5 min. To monitor EPSC amplitude over time, two test responses to a PF pulse (with 50 ms interval) were evoked every 20s in voltage-clamp mode. In LTP experiments, cells were switched to current-clamp mode for tetanization. Paired-pulse ratio (PPR) was calculated as the ratio of the amplitude of the second evoked excitatory postsynaptic current (eEPSC) to that of the first. eEPSC amplitudes and PPR were averaged per minute and normalized for final representation. For the experiments on intrinsic excitability recordings were performed in current-clamp mode, again using an EPC-10 amplifier (HEKA Electronics). Intrinsic excitability was monitored through injection of brief steps (550 ms) of increasing depolarizing current (20 steps from 50 to 1000pA). The spike count was taken as a measure of excitability. Input resistance (R_i) was measured by injection of hyperpolarizing test currents (200 pA; 100 ms) and was calculated from the voltage transient toward the end of current injection. Recordings were excluded if the input resistance varied by $> 20\%$.

Single channel activity was measured in cell-attached configuration with pipettes between 6-8 M Ω of resistance, containing the same intracellular solution used for whole cell recordings but containing 100 μ M of S-AMPA (Tocris). After reaching a patch resistance above 2 G Ω , the patch voltage clamp was decreased from close to resting potential (-60 mV approx.) to twice as negative (-120 mV approx.). In this configuration the ionic driving force across the channel was reversed and therefore the openings produced depolarizing events in the patch pipette. To determine the actual driving force across the AMPAR we broke into whole cell mode after the single channel recording was acquired and measured the cell resting potential. The driving potential resulted from the subtraction of the cell resting potential to the clamped voltage, and this value was used to later on calculate the receptor conductance. To further corroborate that the openings observed were caused by AMPARs, a subset of channels were also recorded at close to resting potential voltages (-60mV) and at 0mV. When clamped at close to cell resting potential, the driving force across the channel is minimal and the openings are no longer visible. When clamped at 0mV the driving force is reversed and the events detected by the pipette are of similar size but hyperpolarizing (not shown), being fully consistent with AMPARs behavior.

For the outside-out patches AMPA responses, pipettes with 4-6 M Ω resistance were approached to PC soma until establishing a Gigaseal (1 G Ω resistance). After compensating the capacitance artifact, we let the seal rest until it reached resistances above 2 G Ω . After breaking into whole cell mode, the pipette was slowly

retracted until both the cell and the outside-out patch were re-sealed again. Every 20 seconds a 100ms puff of 100 μ M AMPA was delivered with a Picospritzer III (Parker, Hollis, USA) to generate an AMPA dependent response. In each sweep, a 100ms depolarizing test pulse (-10 mV) was applied in order to test series resistance and membrane capacitance. Only patches with a constant resistance over 1 G Ω were considered for analysis. Membrane capacitance used to control for outside out patch size assuming a specific membrane capacitance of 0.01 pF per 1 μ m² (Schmidt-Hieber and Bischofberger, 2010). Our patches presented comparable estimated areas of 12.1 \pm 0.9 and 11.8 \pm 0.8 μ m² in control and 8-CPT containing patches respectively ($p=0.42$).

Drugs and pharmacology

For mEPSC recordings, tetrodotoxin (TTX, 1 μ M, Sigma) was added to the bath solution to block network activity in order to only measure excitatory spontaneous release. In order to isolate the specific contribution of AMPA and kainate receptors to glutamatergic transmission in WT and KO mice, the AMPA specific blocker GYKI52466 (30 μ M, Sigma) or the kainate specific blocker SYM2081 (5 μ M, Sigma) were added to the extracellular bath solution. For the pharmacological investigation of the cAMP-GluA3 dependent pathway the following membrane permeable drugs were added to the bath of ACSF: 50 μ M Forskolin (adenylyl cyclase activator, Sigma), 20 μ M H89 (PKA antagonist, Tocris), 5 μ M KT5720 (PKA antagonist, Sigma), and 10 μ M ESI-05 (EPAC antagonist, BioLog). In addition, we applied the membrane non-permeable agonist for EPAC, 8-CPT-2Me-cAMP (20 μ M, Tocris Bioscience) to the intracellular whole cell recording solution to investigate the postsynaptic impact of EPAC. In order to obtain a monophasic time decay of the AMPA-evoked responses in outside-out patches we added a final mixture of 80 μ M PEPA (AMPA flop splice variant desensitization blocker, Tocris bioscience) and 100 μ M cyclothiazide (CTZ, AMPAR flip splice variant desensitization blocker, Tocris bioscience) to the bath solution.

Electrophysiology data analysis

Spontaneous mEPSC and evoked EPSC recordings were analyzed with MiniAnalysis software (Synaptosoft) and ClampFit (Molecular Devices), respectively. To calculate τ_{fast} (fast desensitizing component) and τ_{slow} (slow non-desensitizing component) of AMPA evoked currents in outside-out patches a double exponential function was fitted using ClampFit with DC offset set at 0. The decay of the averaged current was fitted to the following equation: $I = A_1 e^{-t/\tau_1} + A_2 e^{-t/\tau_2}$. In this equation τ_1 represents τ_{fast} . The percentage of the decay represented by the slow component

(% _{slow}) was calculated by the function $A1/(A1+A2)$, as described elsewhere (Christian et al., 2013). The weighted decay time constant for AMPA evoked currents in outside-out patches in the presence of desensitization blockers was calculated by dividing the total charge transfer (in fC) by the peak amplitude (in pA). Non-stationary fluctuation analysis of outside-out patches traces was carried out following previously described methods (Alvarez et al., 2002; Benke et al., 2001; Hartveit and Veruki, 2007). In short, peak aligned AMPA evoked currents recorded over 10-15 sweeps per outside-out patch were binned in 10 equally sized bins of 150 ms each and for each bin the mean amplitude and variance were calculated. The data distribution resulting after plotting amplitude versus variance was fitted with the following equation: $\sigma^2 = iI - \frac{I^2}{N} + \sigma_b^2$, where the variance (σ^2) of the amplitude of the current (I) obtained at each time point is explained as a function of the single unitary current (i) and the number of functional conducting channels (N) with an offset given by the variance of the baseline noise (σ_b^2). The number of functional channels was extracted from the derivative at $I = 0$, and the single channel conductance was calculated by dividing the unitary current by the applied voltage with respect to the reversal potential ($V_{\text{holding}} - E_{\text{reversal}}$, -70 mV and 0 mV, respectively). The peak open probability (P_0), which corresponds to the fraction of available functional channels open at the time of the peak current (I_{peak}), was calculated from the following equation: $P_0 = I_{\text{peak}}/N_{\text{max}}$. In this equation N_{max} represents the theoretical maximum of available channels opened at the point where the theoretical maximum amplitude reaches the minimum variability (σ_b^2) in the given parabola fit.

Single channel activity was analyzed using ClampFit (Molecular Devices). Three detection thresholds were used to detect O1 (1.5pA), O2 (3pA) and O3 (4.5pA) openings in single channel AMPA receptors in steady baseline recordings (no holding current fluctuations). Events with latency shorter than 0.3 ms were ignored to prevent noise to be recognized as openings.

In vitro 2-photon imaging

Organotypic cerebellar slices were made from P7-9 mice using a protocol adapted from previous studies (Hurtado de et al., 2011; Stoppini et al., 1991) and kept in culture 4-7 days prior to the experiments. Slices were then transfected with sindbis virus expressing rat flip GluA3 AMPAR fused to the pH sensitive version of GFP Super Eccliptic pHluorophor (GluA3-SEP) for a period of 24-48 hours prior to the imaging session.

For imaging, slices were transferred from the incubation solution to the recording chamber containing ACSF (same composition as mentioned before but with 4 μ M calcium and 4 μ M magnesium). Three-dimensional images were collected on a custom-built two-photon microscope based on a Fluoview laser-scanning microscope (Olympus). The light source was a mode-locked Ti:sapphire laser (Chameleon, Coherent) tuned at 850 nm using a 60x objective. Optical sections were captured every 1 μ m from transfected PC dendrites. Fluorescence intensity was quantified from projections of stacked sections using ImageJ software (NIH).

Immunohistochemistry

Seven wild-type littermate mice received an overdose of sodium pentobarbital via IP injection and were perfused intracardially with 50 ml of oxygenated ice cold slicing solution with (n=3) or without (n=4) 50 μ M forskolin, followed by 60 ml of fixative (4% paraformaldehyde in 0.1 M PB, pH7.6) at a rate of 5.5 ml/min. Brains were carefully removed from the skull and post-fixed for a maximum of 2 hours in the same fixative solution at 4°C. Then, they were immersed in 30% sucrose in PB at 4°C until they sank, and 40 μ m thick frontal sections obtained with a freezing microtome were collected into four matching series. For surface GluA2 detection, the slices were previously incubated in blocking solution containing 10% horse serum in PB 0.1 M to minimize non-specific binding of the antibodies. After 1 hour, blocking solution was replaced by the primary antibody solution containing 5% horse serum in 0.1M PB, mouse anti-GluA2 antibody (Chemicon, Millipore) at a concentration of 1:200 and rabbit anti-SCN2B (Abcam Ltd) at a concentration of 1:1000 as internal control for 48 hours at 4°C. After several rinses with 0.1 M PB slices were incubated overnight in a solution containing 5% horse serum in 0.1 M PB and horse anti-mouse combined with Alexa 594 and horse anti-rabbit combined with Alexa 488 secondary antibodies, both at a concentration of 1:200. After several rinses, slices were mounted and covered with Dako mounting medium (Dako), and imaged under a confocal microscope (Leica SP5). All images were acquired with the same settings and the analysis was performed with ImageJ. For analysis, the fluorescence intensity of equally sized ROIs of the molecular layer of the cerebellum or hippocampus was extracted and normalized to the intensity of a neutral control staining that was not altered by cAMP-dependent pathways.

In Vivo electrophysiology

Mice (males, 4-6 month old) were prepared for chronic experiments as described previously (Wulff et al., 2009). In short, under general anesthesia a pedestal with a

magnet was placed on the frontal and parietal bones of the animal, and a recording chamber was constructed around a small craniotomy in the left occipital bone. After 2 days of recovery, animals were habituated in the setup for 20 min for two days. During the experiments, the animals were alert and immobilized in a custom restrainer. Extracellular activities were recorded with glass micropipettes filled with 2M NaCl solution and advanced into the cerebellar cortex from the surface of Crus I and II. Electrode signals were filtered, amplified and stored for off-line analyses (Spike2, CED, and Cambridge, UK). PCs were identified by the occurrence of both simple spikes and complex spikes, and single-unit activity was confirmed by a brief pause in simple-spike firing following each complex spike (i.e. climbing fiber pause; see De Zeeuw et al., 2011). The whole field visual stimulation was presented by rotating a cylindrical screen (diameter 63 cm) with a random-dotted pattern (each element 2°) at 0.6 HZ with amplitude of 5°. Offline analysis was conducted in Matlab (Mathworks, Natick, MA, USA). CV2 of simple spikes was calculated as the mean value of $(2 \times (IS_{In+1} - IS_{In})) / (IS_{In+1} + IS_{In})$ (Wulff et al., 2009). Modulation of simple spikes and complex spikes was calculated as the amplitude of the sine wave fitted to the histogram of spike rate. Statistical analysis was done using Student's t-test with SPSS (IBM Corporation, Armonk, NY, USA).

REFERENCES

- Alvarez,O., Gonzalez,C., and Latorre,R. (2002). Counting channels: a tutorial guide on ion channel fluctuation analysis. *Adv. Physiol Educ.* 26, 327-341.
- Benke,T.A., Luthi,A., Palmer,M.J., Wikstrom,M.A., Anderson,W.W., Isaac,J.T., and Collingridge,G.L. (2001). Mathematical modelling of non-stationary fluctuation analysis for studying channel properties of synaptic AMPA receptors. *J. Physiol* 537, 407-420.
- Christian,C.A., Herbert,A.G., Holt,R.L., Peng,K., Sherwood,K.D., Pangratz-Fuehrer,S., Rudolph,U., and Huguenard,J.R. (2013). Endogenous positive allosteric modulation of GABA(A) receptors by diazepam binding inhibitor. *Neuron* 78, 1063-1074.
- Cossart,R., Epsztein,J., Tyzio,R., Becq,H., Hirsch,J., Ben-Ari,Y., and Crepel,V. (2002). Quantal release of glutamate generates pure kainate and mixed AMPA/kainate EPSCs in hippocampal neurons. *Neuron* 35, 147-159.
- de Jeu,M., and De Zeeuw,C.I. (2012). Video-oculography in mice. *J. Vis. Exp.* e3971.
- Hartveit,E., and Veruki,M.L. (2007). Studying properties of neurotransmitter receptors by non-stationary noise analysis of spontaneous postsynaptic currents and agonist-evoked responses in outside-out patches. *Nat. Protoc.* 2, 434-448.
- Hurtado de,M.T., Balana,B., Slesinger,P.A., and Verma,I.M. (2011). Organotypic cerebellar cultures: apoptotic challenges and detection. *J. Vis. Exp.*
- Kerchner,G.A., and Nicoll,R.A. (2008). Silent synapses and the emergence of a postsynaptic mechanism for LTP. *Nat. Rev. Neurosci.* 9, 813-825.

Linden,D.J. (2001). The expression of cerebellar LTD in culture is not associated with changes in AMPA-receptor kinetics, agonist affinity, or unitary conductance. *Proc. Natl. Acad. Sci. U. S. A* 98, 14066-14071.

Saab,A.S., Neumeyer,A., Jahn,H.M., Cupido,A., Simek,A.A., Boele,H.J., Scheller,A., Le,M.K., Gotz,M., Monyer,H., Sprengel,R., Rubio,M.E., Deitmer,J.W., De Zeeuw,C.I., and Kirchhoff,F. (2012). Bergmann glial AMPA receptors are required for fine motor coordination. *Science* 337, 749-753.

Schmidt-Hieber,C., and Bischofberger,J. (2010). Fast sodium channel gating supports localized and efficient axonal action potential initiation. *J. Neurosci.* 30, 10233-10242.

Stahl,J.S., van Alphen,A.M., and De Zeeuw,C.I. (2000). A comparison of video and magnetic search coil recordings of mouse eye movements. *J. Neurosci. Methods* 99, 101-110.

Stoppini,L., Buchs,P.A., and Muller,D. (1991). A simple method for organotypic cultures of nervous tissue. *J. Neurosci. Methods* 37, 173-182.

Yan,D., Yamasaki,M., Straub,C., Watanabe,M., and Tomita,S. (2013). Homeostatic control of synaptic transmission by distinct glutamate receptors. *Neuron* 78, 687-699.